The application of Electrical Resistance Tomography within a vacuum sugar pan in order to better understand its boiling dynamics

Daniel Sanderson

A dissertation submitted to the School of Electrical, Electronic & Computer Engineering,

University of KwaZulu Natal, in fulfillment of the requirements for the degree of Master of Science in Engineering.

I ..... declare that

(i) The research reported in this thesis, except where otherwise indicated, is my original work.

(ii) This thesis has not been submitted for any degree or examination at any other university.

(iii) This thesis does not contain other persons' data, pictures, graphs or other information, unless specifically acknowledged as being sourced from other persons.

(iv) This thesis does not contain other persons' writing, unless specifically acknowledged as being sourced from other researchers. Where other written sources have been quoted, then:

a) their words have been re-written but the general information attributed to them has been referenced;

b) where their exact words have been used, their writing has been placed inside quotation marks, and referenced.

To my wife

Acknowledgements

The most sincere of thanks must go out to all the people who have contributed to the completion of this research:

- Dr Leigh Jarvis, my supervisor, for the endless meetings and constant guidance, for helping point me in the right direction
- Dr Dave Love for arranging access to the mill, and for the constant input into the mechanical designs that were needed to overcome collar displacement within the pan
- Dr Steve Davis for his contribution to understanding the boiling process
- The workshop staff at UKZN for helping implement the designs, specifically, Mr Antony Lester for his helpful insight and selflessly giving up his time for me
- My wife for putting up with an academic husband!
- SMRI/THRIP, without whose sponsorship this research would not have been possible

Please note that the contents of this dissertation are considered confidential.

Abstract

This dissertation is concerned with the application of tomography within the sugar industry; in particular non-accessible locations found in a sugar mill. In this study, the focus of research is that of a vacuum pan, and if better understood through tomographical techniques could significantly improve mill efficiency and throughput. The tomography system comprises unique mechanical interfaces, data acquisition modules and software algorithms in order to generate images which reflect the dynamics in the tomographical sensor zone.

The distribution of gas (low conductivity) and liquid (high conductivity) within a tube is of main interest in order to understand the boiling dynamics and ultimately pan design. This is attained by determining the internal cross-sectional spatial distribution of conductivity of a number of tubes within the pan simultaneously. Thermal properties of the contents of the sugar pan (a syrup-like substance known as massecuite) at different boiling stages can be estimated based on the tomographical data.

Data acquisition is achieved via an in-house designed electronic state machine. A neighbourhood back-projection reconstruction technique was developed in MATLAB in order to generate tomographical images.

Results from the system have identified different boiling dynamics which improve the understanding and design of vacuum sugar pans.

Table of Contents

List of Figures

1. Introduction

Tomography is a technique of creating an image, or 'tomograph' by sectioning through the use of a wave of energy. It has been developed recently in order to better understand the internal dynamics of enclosed objects, or 'phantoms'. The images are created by injecting currents to the periphery of the phantom and applying a mathematical reconstruction algorithm to the subsequent voltage data on adjacent electrodes.

Tomography has been primarily developed for use in the medical industry, where the imaging of a patient's internal body structure without invasiveness is extremely desirable. However, this is the first time it has been applied to massecuite in a sugar mill.

1.1 Various Tomographical Techniques

There are several different methods of obtaining tomographical images [**1**], including:

1.1.1 X-rays, gamma rays and magnetic resonance imaging

X-rays, gamma rays and magnetic resonance imaging techniques are all examples of tomography.

Computer Aided Tomography Scans (CAT scans) are medical imaging systems which are used to create tomographical images using computer processing power. In CAT Scans, X-rays are used in producing images as they travel in straight lines through a body and are then detected by sensors. When an X-ray comes into contact with a dense medium such as bone tissue, it is attenuated. X rays have excellent spatial resolution; however they also have the unfortunate side effect of causing cancer.

Gamma rays are released when radiopharmaceuticals undergo radioactive decay. Radiopharmaceuticals are introduced to a body to concentrate on target organs. These gamma rays cause light flashes on nearby scintillation crystals, and a photo detector can produce images of the radiopharmaceutical.

Magnetic resonance imaging (MRI) can produce images of certain chemicals, for example, hydrogen concentration in water. A strong magnetic field is passed through a patient and the

precession [1]of the hydrogen atoms is monitored with an oscillating electric field[**1**]. This yields the spatial distribution with great clarity; however it is very large and expensive.

[1] Precession occurs when a rotating body changes its axis of rotation, in this case due to presence of the magnetic field.

1.1.2 Electrical Capacitance Tomography (ECT)

In ECT the electrodes detect variances in the dielectric properties of the medium within the phantom, or capacitance. Electrodes and data acquisition hardware need to be extremely sensitive as these changes occur on the micro- or pico-Farad level, and hence ECT is useful in applications where non-conductive mediums are being tomographied. These sensitivity requirements enforce delicate electronic hardware design, as well as very short cable lengths.

1.1.3 Electrical Resistance Tomography (ERT)

In ERT the conductive properties of a medium are ascertained by injecting currents through electrodes situated on the boundaries of the phantom. Differential voltage readings are taken from the other electrodes, and from these readings a potential distribution map is generated.

There are several different methods by which the current may be injected into the phantom, and the tomography Research Group at UKZN has successfully implemented two, namely Adaptive and Neighbourhood tomography. Currently work is also being done on an Opposite injection scheme.

1.1.3.1 Adaptive Method

Adaptive tomography is a method which utilizes an adaptive data collection algorithm, where a current distribution can be manipulated to any desired format by injecting an appropriate magnitude current through every electrode simultaneously bar one, which is used as a common ground. Each electrode can provide a bipolar current within a specified range, and voltages are set up with respect to the common ground. The current is constantly altered by an algorithm as the sensitivity is measured in the phantom until a situation where the electric potential at all points within the phantom are equal for a homogenous medium. This is known as the optimum current distribution. Thus, for a 16-electode system, 16 current sources are required [**2**], [**3**].

Figure 1-1 shows how, for an adaptive injection scheme, the current amplitudes must follow a cosine curve in order to obtain a distribution which is perfectly uniform. The adaptive method offers the greatest distinguishability and is extremely versatile; however it is somewhat more complex in implementation in that setting up the individual current sources so that they are perfectly matched is a tedious task and would be difficult to achieve. Also, the supplementary information from the additional current sources forces the reconstruction algorithm to become much heavier computationally [**4**], [**5**].

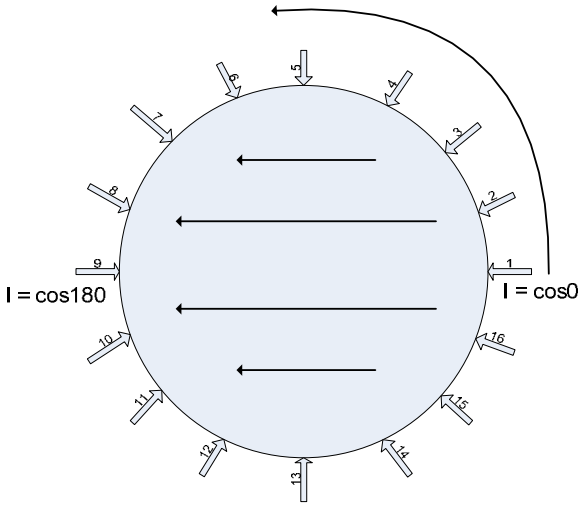

Figure 1-1: Adaptive tomography injection scheme

1.1.3.2 Neighbourhood Method

The Neighbourhood method utilizes a technique whereby a single current source is used and is multiplexed through to the correct electrodes. Compared to Adaptive tomography it is computationally less expensive and significantly lighter on component count when designing the governing electronic state machine.

To build up the image, a circular model of a two-dimensional transverse plane is simulated. When current is injected between two neighbouring electrodes, a potential distribution is set up which in a homogenous medium will follow a specific pattern, and the expected voltages at all the electrodes can be calculated. If there is a region within the phantom which has a higher resistance than the surrounding medium, the measured voltages will change by factor related to the change in resistivity.

Current is then injected between the next two neighbouring electrode pairs, and voltage measurements are again taken around the ring. The algorithm repeats until injections have been made between every pair. Thus in a 16-electrode tomographical system 16*13 = 208 measurements are taken. Generally, in order to improve accuracy, more measurements will be taken and averaged out to provide a single reading. Figure 1-2shows the injection scheme for a Neighbourhood method.

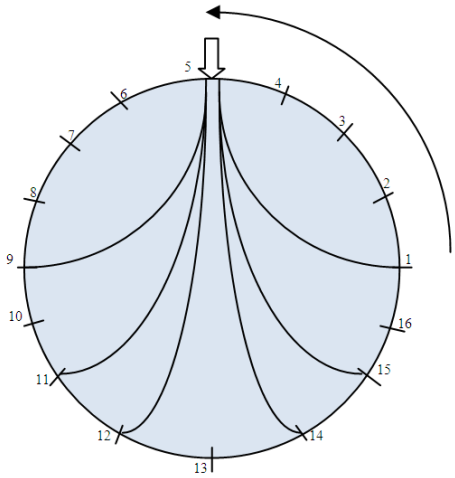

Figure 1-2: Neighbourhood tomography injection scheme

Figure 1-3 shows how the current injection algorithm increments around the periphery of the phantom, and Figure 1-4 shows how an area of high resistivity would be illuminated as the images are superimposed.

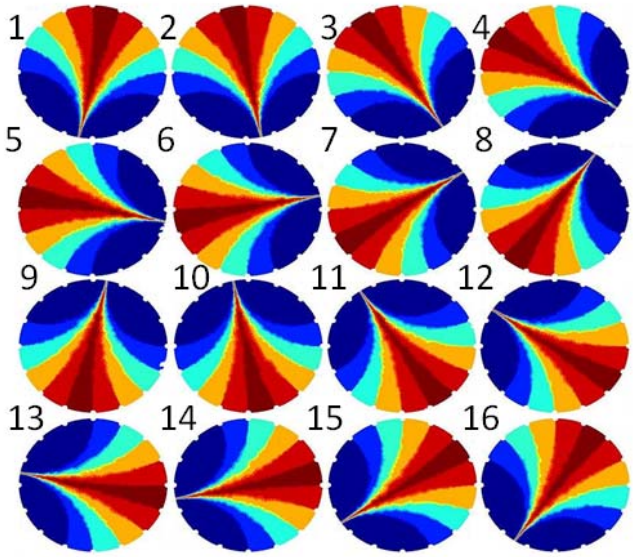

Figure 1-3: Current injection algorithm successively incrementing (1-16) around periphery of homogeneous medium phantom

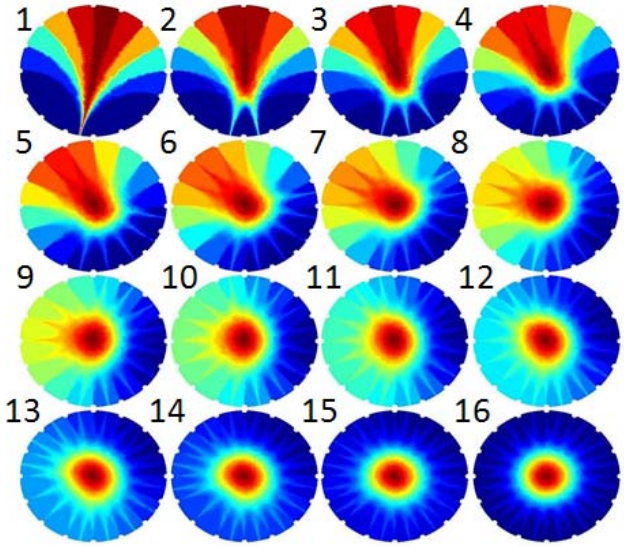

Figure 1-4: Superimposition of successive images to illuminate interior of phantom. Part 16 (bottom right) is the final result presented to the user

The neighbourhood method is the more widely used implementation of tomography due to its robust nature and relative ease of use when compared to the Adaptive method. There are other methods, however, some of which include:

- Opposite method. Current is injected through diametrically opposed electrodes with a voltage reference electrode situated adjacent to the injection electrode. Voltages are then measured on all the remaining electrodes with respect to the reference. Current injection is then rotated to the neighbouring pair of opposite electrodes, and so is the reference electrode. New voltage measurements are then taken with respect to the new reference. The opposite method yields a uniform current density and good sensitivity in the centre of the phantom.

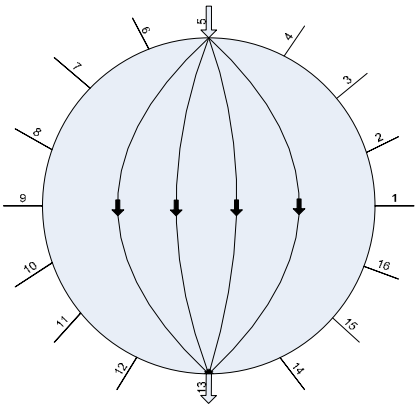

Figure 1-5: Opposite method injection scheme

- Cross method. This method is useful where electrodes are separated by large dimensions, such as when the phantom is of a non-circular shape. A current reference is set up at electrode one and a voltage reference in electrode two. Current is then injected through all of the remaining electrodes successively and upon injecting each current, voltages at all the remaining electrodes are measured except for the current electrodes. The references are then shifted and the process is repeated. Periphery sensitivity is not very good with this method; however the matrix is better conditioned[2].

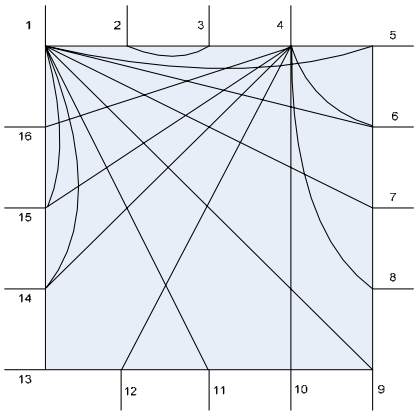

Figure 1-6: Cross method

[2] The conditionality of a matrix indicates the accuracy of the solution to the system after an approximate solution.

- Multi-reference method. Current is injected through multiple electrodes at once and exit through a common ground. This method was a precursor to the adaptive method, and the currents injected were not manipulated by a controller. Figure 1-7.

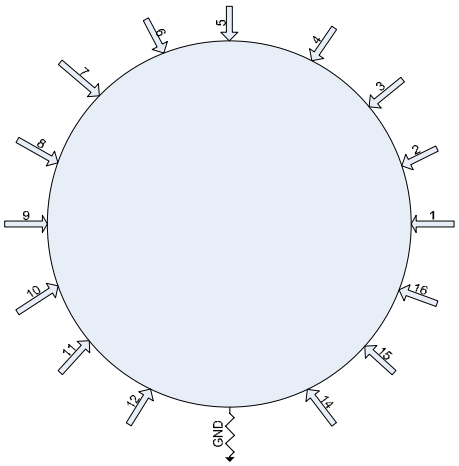

Figure 1-7: Multi-reference method

1.2 Tomography in the Sugar Industry

Sugar cane is grown in tropical and sub-tropical areas. Once harvested, the cane is processed at a sugar mill. The cane is fed through a system of washers, large crushers and roller mills which separate the cane fibre from the sugar juice. The fibres, known as 'bagasse', are then burnt in furnaces in order to produce steam power for the plant. Excess power is sometimes sold off to nearby communities.

The sugar juice at this stage is contaminated with soil and stray fibres and is therefore cleaned in a clarifier, which is a gravitational tank which removes excess solids. The juice is fed with lime ($Ca(OH)_2$) which maintains pH at 7 and prevents decomposition into fructose and glucose, as well as precipitating impurities.

The clear juice exiting the clarifier stage consists of approximately 15% sugar and is passed through a series of evaporators before arriving at the boilers, where the crystals are grown. This is accomplished by creating a high temperature and low pressure environment where the sugar juice is seeded with crystallized sugar and brought to a boil using heated steam pipes. Under these conditions a crystallization process occurs and the crystals 'grow'. The resulting syrup is known as massecuite and is sent to a crystallization tank where it cools down and the crystals continue to mature. The massecuite is then sent to a series of centrifuges where the crystals and liquid (known as molasses) are separated. The liquid is sent back to the pan boilers a further two times, effectively creating 'A', 'B' and 'C' molasses. The 'B' and 'C' molasses which contain dissolved crystal sugars are often used to seed new massecuite.

It is in the vacuum pan boilers where the project has had its primary focus. The critical part of the sugar-making process is crystallization; the crystals are grown within a low-pressure and high temperature environment. However it is extremely important to obtain all the right parameters for the grain: size, separation and colour need to be correct otherwise the crystals may dissolve as they grow, or false grain may develop, which are very small sugar crystals formed by a secondary nucleation in sugar pans, which leads to bimodal crystal size distribution. These small crystals are not the correct size or shape required [**6**].

Not very much is known about the dynamics of pan boiling, and as such it has developed into an art more than a science. Therefore sugar mills rely heavily on the handed-down skills of pan boilers [**7**].

There is a constant need to better understand pan boiling, and what makes a pan boil well. As such the designs are continuously being upgraded and improved upon; many mills contain very old batch pans from the first batch designs right through to present. Some new pans include tall round batch pans as opposed to horizontal, or two pans which sit one atop the other, split into slices. As new designs are introduced, care must be taken not to interfere with the circulation of massecuite within the pan, which is the crucial factor of pan design. If the circulation is poor the pan will not boil properly; boiling times will increase, throughput will drop, crystal quality will be poor, and false grain will be introduced [**6**].

Until now the only way to monitor the boiling of a pan was to physically look inside the pan through viewing portholes; however these only offer a limited perspective of the internal dynamics – bubbles can be seen to form on top of the massecuite but it has not been possible to individually monitor tubes as they boil. For example, how well is the tube next to the down take boiling vs. the tube at the outside of the pan? Are tubes in a new design boiling more efficiently than tubes in an old design? When steam is applied to the system, does the boiling visibly improve? If such questions could be better answered, much could be done to improve the efficiency of sugar mills.

By taking a tube and putting electrodes around it, the electrical properties of the massecuite within the tube can be measured, in turn providing a cross-sectional image of the top of the tube. The size of bubbles, speed of bubbles, and number of bubbles can be determined.

1.3 Structure of this dissertation

Chapter 2 describes the theory of tomography, in particular the reconstruction algorithms used to generate the images obtained in this research.

Chapter 3 deals with the problem requiring the research, and the subsequent argument for the methods chosen to implement the hardware.

Chapter 4 describes the implementation of the design, with a detailed hardware description and its operation.

Chapter 5 presents the results obtained and discuss the performance of the system as a whole.

Chapter 6 shows the work done on creating a real-time tomography system, followed by a conclusion of the dissertation.

2. A Theory of Tomography

Tomography is more complicated to implement when compared to other imaging techniques such as X-rays because the electrical current is not confined to a narrow beam when injected into the phantom; but rather spreads out over the entire region. This makes it more difficult to implement and more prone to accuracy errors. This chapter will describe the theory behind the forward and inverse problems, and their application to ERT.

2.1 Introduction

ERT images are generated by determining the resistivity distribution within a phantom when an electric current is applied to it. The resulting electric field set up within the phantom is governed by Poisson's equation [**1**]:

$$\nabla . \rho^{-1} \nabla V = f \tag{2.1}$$

This electric field has the following boundary conditions:

$$V = V_0 \text{ on } \partial A \tag{2.2}$$

$$\rho^{-1} \frac{\partial V}{\partial n} = J_0 \text{ on } \partial A \tag{2.3}$$

where V, f and ρ are the Voltage, current distributions and resistivity within the phantom being tomographied, and V_0 and J_0 are the voltage and current densities at the boundary. In ERT AC currents are used to generate a map of the spatial conductivity distribution. Because there are no AC current sources within the phantom, i.e. $f = 0$, Equation 2.1 becomes

$$\nabla . \rho^{-1} \nabla V = 0. \tag{2.4}$$

2.2 The Forward and Inverse Problems

In ERT the boundary voltages and currents are known and it is desired to compute ρ^{-1}; this is known as solving the inverse problem; the converse to this is the forward problem, where ρ is known and the boundary voltages and currents are required. Typically, in order to solve the inverse problem iterative solutions of the forward problem must be solved, i.e. continuously update ρ until the calculated voltages and currents match those measured. When this occurs it can be assumed that the calculated spatial conductivity distribution within the phantom is an accurate description of real life [**8**].

A general analytical solution to Equation 2.4 is impossible, hence a numerical method is employed – the Finite Element Method (FEM). This involves converting Equation 2.4 (a calculus problem) into a linear algebraic problem, which is more easily solved.

The region of interest, or phantom, can be discretized into a finite number of triangular elements in which the conductivity can be specified. If the medium within the phantom is assumed to be homogeneous and isotropic, then Equation 2.4 can be expressed as

$$v = Yc \tag{2.5}$$

where v is a vector of voltage measurements obtained at the periphery, c is a vector of conductivity values, and Y is a transformation matrix.

The conductivity values are unknown and the periphery voltages are known, and so the desired solution is:

$$c = Y^{-1}v \tag{2.6}$$

hence the measurements taken at the periphery are formed into a vector and applied to a transformation matrix to obtain c, which is the inverse problem. However, Y is a non-linear transformation and as such cannot be inverted by standard matrix techniques. It can then be assumed that for small variations, Y can be approximated as linear and then inverted, however this solution becomes error-prone. A smaller mesh size can reduce this error significantly; however the transformation matrix Y becomes correspondingly larger, resulting in increased computational time and processing power requirements. A compromise for this constriction is to have a small mesh size where there are larger conductivity changes and larger mesh sizes where the conductivity changes are small. Essentially this means that the ERT system is more sensitive

at the periphery of the phantom and less sensitive in the middle. A 16-electrode mesh model is shown in Figure 2-1.

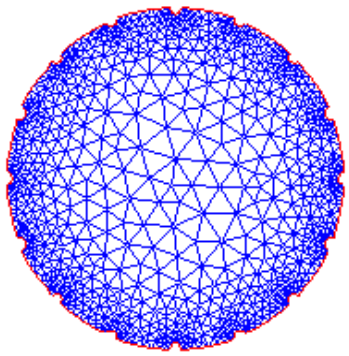

Figure 2-1: Mesh model for a 16-electrode system

2.3 Newton-Raphson Method

The Newton-Raphson iteration method is the most commonly used in ERT. It minimizes the mean square difference between values simulated in a model and measured voltages until the error falls within a predefined limit. This difference is termed the 'objective function':

$$\Phi(\rho) = \left(\frac{1}{2}\right)(f(\rho) - V_0)^T(f(\rho) - V_0) \tag{2.7}$$

where $f(\rho)$ is the estimated voltage for a conductivity distribution ρ, V_0 is the measured voltage, and T is to transpose.

It is now required to find a ρ which will minimize the divergence criterion of the objective function, i.e. Φ. Therefore its derivative is set to zero:

$$\Phi'(\rho) = [f'(\rho)]^T(f(\rho) - V_0) = 0 \tag{2.8}$$

where $f'(\rho)_{ij} = \frac{\partial f_i}{\partial g_j}$ and is termed the Jacobian matrix and contains partial derivatives of the calculated voltages with respect to the conductivity distribution.

There are various methods for calculating the Jacobian, but the fundamental process requires the determination of variances in periphery voltages according to changes in conductivity. Individual elements in the Finite Element Mesh are varied in order to solve the forward problem iteratively as the Jacobian is constructed.

The first linear terms of the Taylor expansion of $\Phi'(\rho)$ are taken around a point ρ^k to achieve

$$\Phi'\left(\rho^{k+1}\right) \approx \Phi'\left(\rho^k\right) + \Phi''(\rho^k)\Delta\rho^k \tag{2.9}$$

where$\rho^{k+1} = \rho^k + \Delta\rho^k$.

Φ'' in Equation 2.9 is the Hessian matrix:

$$\Phi'' = [f']^T f' + [f'']^T\{I \otimes [f - V_0]\} \tag{2.10}$$

however the second term is significantly less than the first and *f''* is excessively complex to calculate, therefore:

$$\Phi'' = [f']^T f' \tag{2.11}$$

The conductivity update $\Delta\rho^k$ in Equation 2.9 can then be simplified to

$$\Delta\rho^k = -\frac{[f'(\rho^k)]^T[f\left(\rho^k\right) - V_0]}{[f'(\rho^k)]^T \cdot [f'(\rho^k)]} \tag{2.12}$$

The initial conductivity guess ρ is updated by $\Delta\rho^k$ until the objective function $\Phi(\rho)$ falls within the stopping criterion, which is usually the measurement noise of the system.

The Hessian matrix is often an ill-conditioned one, meaning that small numerical changes during calculation can have drastic effects on the result (rounding off is a common example), which can make the inverse problem difficult to calculate accurately and extremely sensitive to accumulative errors. To normalize the Hessian all elements of the matrix are multiplied by $1/\sqrt{h_{ii}}$, to become $(\Phi'')^{\mathrm{T}}$, forcing the diagonal elements to unity. The normalized Hessian is then smoothed by adding a factor ω_n to all the diagonals. Therefore Equation 2.12 becomes

$$\Delta\rho^k = -\left\{\frac{[f'(\rho^k)]^T[f\left(\rho^k\right) - V_0]}{\{[f'(\rho^k)]^T \cdot [f'(\rho^k)]\} + \omega_n I}\right\} \tag{2.13}$$

with I representing the identity matrix.

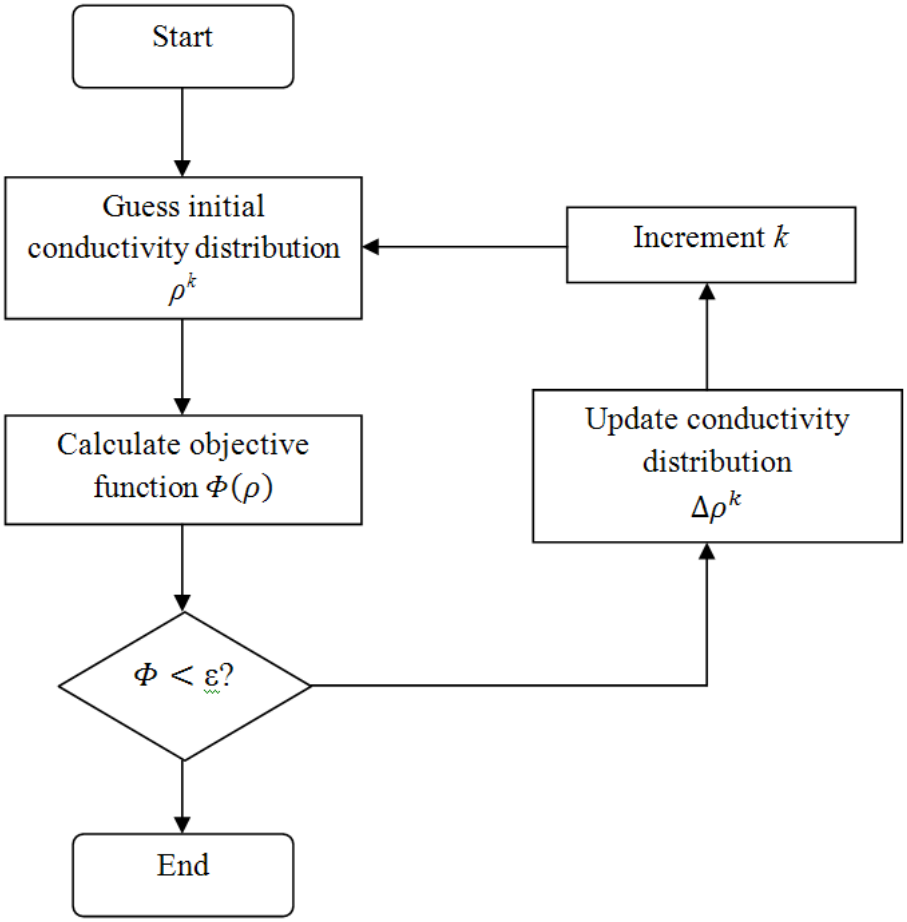

Figure 2-2: The Newton-Raphson method iterates *k* times in order to minimise Φ

This algorithm is well suited for the Neighbourhood Data Collection method and produces a fast mathematical implementation .

3. Problem and Argument

Within a sugar mill there are several regions of interest, as has been discussed previously in Chapter 1. Tomography applications have been identified in two areas within the Sugar Industry - clarification of the 'sugar juice' and the growing of sugar crystals.

3.1 Two problems – Clarifier and Vacuum Sugar Pan

The clarifier, where raw liquid from the crushed cane is separated from sediment and stray fibres, is a large vessel within the sugar mill and is often injected with a lime solution ($Ca(OH)_2$) to maintain pH and help with the separation. In designing a clarifier, the main aim is geared towards determining flow solutions which will speed up the clarification process, as well as reduce the sugar content in the separated sediment. Traditionally, clarifier design is accomplished by combining past designs and experience with Computer Fluid Dynamics (CFD) modelling packages, which serve to provide the designer with a theoretical outcome of the flow characteristics within a particular design.

The vacuum sugar pan is an extremely harsh environment which operates under vacuum and high temperatures. The aim of the project was to investigate the possibility of introducing tomographic sensors into the environment which could monitor boiling within the pan, specifically the behaviour of different regions of the pan under different conditions. The tomographical input could then give pan designers practical feedback on whether the pan is boiling uniformly or not, as a non-uniform boil can result in uneven grain being developed.

The aim of these investigations was to introduce the concept of tomography to the sugar industry, and show that it can be used as an aid or tool to validate theoretical CFD findings. Once a design has been validated, the designer can manipulate characteristics such as flow conditions in his models, thereby increasing the efficiency of his designs.

Improved Clarifier and Vacuum Pan Boiler designs can add a direct financial advantage to any sugar milling plant, as ultimately better designs result in an increase in annual sugar yield, thereby making the mill more competitive in today's ever growing markets.

3.2 Clarifier Project

Initial research done at UKZN into applying tomography to a clarifier indicated that an adaptive approach should be used as opposed to a neighbourhood method, as it yields a more accurate result (albeit at the cost of complexity) due to the size of the clarifier chamber. Because the dynamics within the chamber are also an unknown quantity, a solution which was as accurate as possible was desired.

Because of the size of a clarifier, it was not practical to implement a tomography system on a full-scale mill version, and a scale model was implemented in the laboratory. An adaptive method of tomography was used in this approach as it yields a more accurate result, which requires individual current sources for each electrode, and a common ground.

The clarifier project, although successfully implemented within the laboratory was deemed unsuitable for full-scale implementation. The clarifier itself is large (typically around $30m^2$), and the nature of an adaptive tomography device requires current sources to be as close as possible to the electrodes.

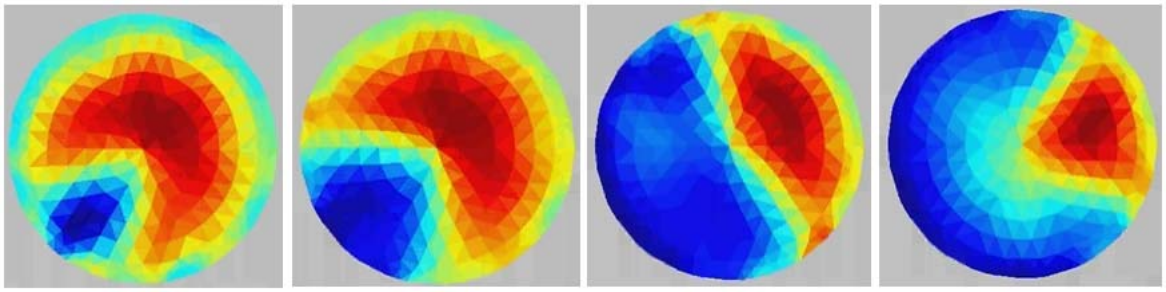

Figure 3-1: Diffusion experiment using an Adaptive technique

Figure 3-1 presents a test diffusion experiment done by the Research Group at UKZN, where a saline solution (blue) was added to water. [**9**].

3.3 Vacuum Sugar Pan

Massecuite is the product of the centrifuge process of the mill and is essentially thick syrup containing approximately 60% weight of sucrose. It is seeded with crystalline sugar and under certain conditions will begin to boil, facilitating growth of the crystals. The essential factor in this boiling process is circulation within the pan, which serves to aid in heat transfer and prevent stagnant spots within the pan which would result in an uneven rate of crystal growth. Figure 3-2 shows various crystals under different development stages; note the rounded edges in (b) and (c)

compared to the sharp and well-defined edges and corners of (a) and (d) which are the desired shape. These images were taken at the Maidstone Sugar Mill in July 2008.

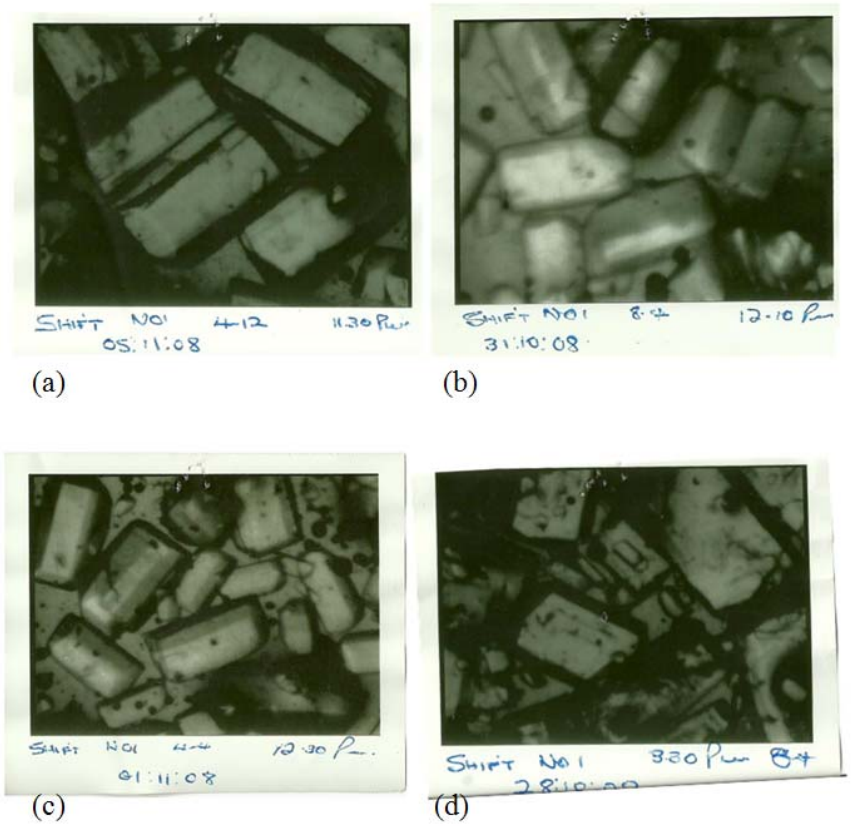

Figure 3-2: Sugar crystals at different stages of boiling

The impedance of the massecuite contains both a real and an imaginary component and is dependent on the frequency of the signal applied to it. The resistance, or real component, increases with frequency, however the capacitive or imaginary component decreases. If an object is capacitive the voltage across it cannot change instantaneously; which implies time is required for an AC wave to 'settle'. This means that the time taken for the signal applied across the electrodes takes longer to settle, hence decreasing the available time to take an accurate voltage reading.

A vacuum pan has many different designs; the one in question was the common 'batch' pan. Access to the inside of the pan is either through a 'man-hole' or smaller portholes situated in the wall of the pan; a steel jig was constructed which replaced the glass normally in one of the

portholes and the vacuum was sealed using an O-ring. Cabling could then be fed through holes drilled in the jig to service the tomography collars within the pan.

The electronics which govern a tomography system are extremely sensitive to noise, and inherently difficult to calibrate, even within a simulated laboratory environment. As the environment within a sugar mill is heavily industrial, a system which is as robust as possible needs to be implemented. In our neighbourhood tomography system a single current is used, hence there is no pressure for a number of different current sources to be perfectly matched compared to the adaptive method which requires a number of independent 'matched' current sources. Hence a neighbourhood injection method has fewer modular components (meaning there are fewer things which can break!)

An adaptive method also requires a greater deal of processing power by virtue of its computational complexity. An advantage to the adaptive system is that it has a better resolution over the same area than its neighbourhood counterpart, however in the situation of pan boiling it is only desired to know whether a particular tube is boiling, not boiling, or partially boiling. As greater clarity than that is not required, it was decided to implement a neighbourhood method for the pan project.

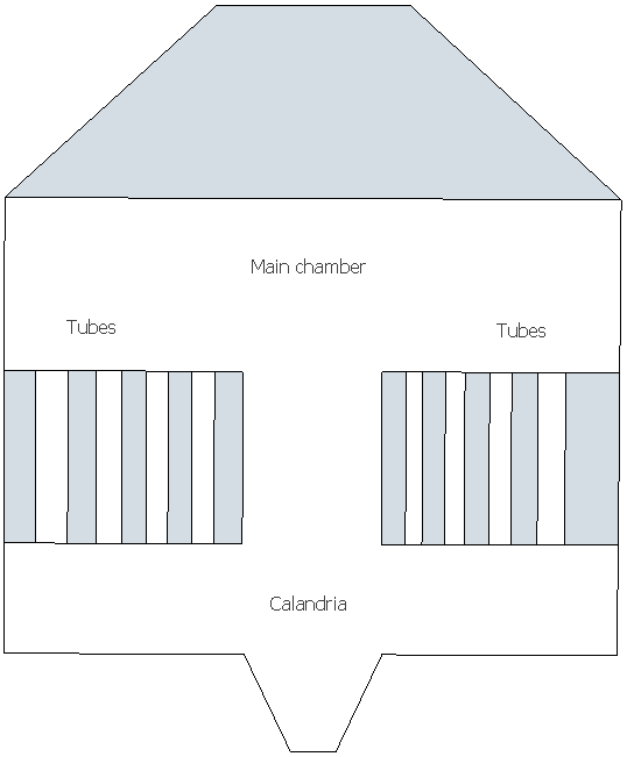

Figure 3-3: Cross-sectional view of vacuum sugar pan

Figure 3-3 shows a simplified view of the internal structure of a sugar pan. As massecuite boils, it is circulated throughout the pan. As it flows up through the calandria tubes it is heated by steam which flows amongst the tubes. This heat eventually spreads throughout the mass of liquid, and when combined with an appropriately low pressure, crystallization occurs. It is therefore important to know how well the heat is conducting within the tubes – if there is too much vapour (bubbles) there will not be enough conduction, however if there is not enough vapour the thermal conduction will be too rapid and hot spots could occur.

Figure 3-4 shows the external structure of a sugar pan, and Figure 3-5 shows the chamber within the pan. The large hole in the centre of Figure 3-5 is the 'down-take' through which the massecuite circulates and eventually leaves the pan during a strike.

Figure 3-4: Vacuum sugar pan showing access porthole

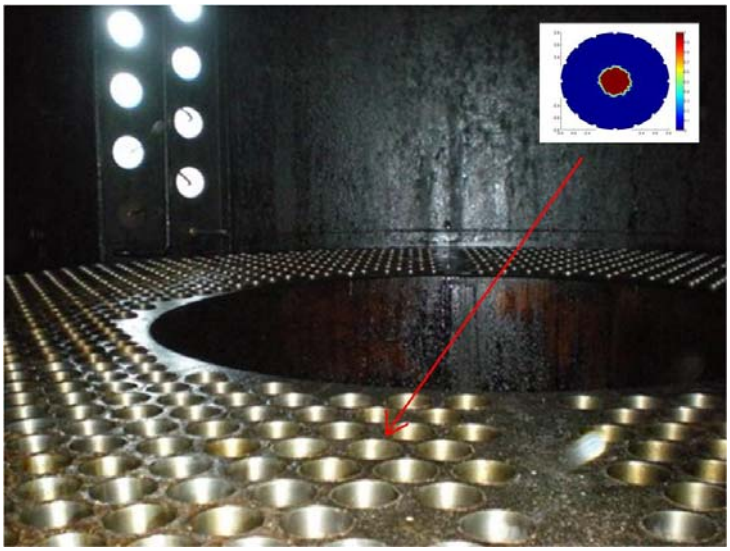

Figure 3-5: Internal structure of pan showing tops of calandria tubes

Heat transfer within the pan is from condensing saturated steam through the tube wall into the massecuite. Most pans have vertical tubes, either stainless steel, steel or brass, 100 mm diameter and 1.5 mm wall thickness, with the steam condensing on the outside, and the condensate running down. The heat is then transferred through the wall into the massecuite. The massecuite

is heated, but boiling is suppressed at the bottom of the tubes due to the hydrostatic head. Higher up boiling takes place, and slugging behaviour results, with the vapour bubbles driving the massecuite upwards out of the tube. This is replaced by fresh massecuite entering the bottom of the tube. The thermal conductivity of the mother liquor is around 0.45 W/(m.K) at boiling temperatures (65-70 ºC, at 15 kPa absolute pressure). The steam is generally supplied at 150 kPa, and 110 ºC.

Initially, the crystal content in the massecuite is low and the massecuite circulates readily, but as crystallisation proceeds and the crystals grow, the viscosity or resistance to flow increases, and boiling is more sluggish. In a batch pan, the level of massecuite also increases, creating a higher hydrostatic head, and reduced boiling. In addition, the higher concentration will increase the boiling point elevation, meaning that the temperature at which the massecuite boils will increase. This all leads to lower heat transfer rates as the pan fills, so the steam addition rate has to be altered to compensate.

3.4 Boiling Mechanics

An empirical approach has led to the design of vacuum pans over the last two centuries, where trial-and-error and 'educated guesswork' has been the main development tool utilized by engineers, due to a lack of detailed information on the operation of these vessels.

Echeverri *et al* [**10**] showed that the viscosity of the massecuite within the vacuum pan determines the nature of the bubbles that can form. Boiling instability can occur within the calandria tubes, which can produce oscillation and vaporisation within the flow. The transfer of momentum from gas to liquid determines the flow present, and as the flow within the tubes (and hence the circulation within the pan as a whole) is critical to the production process, the complex multi-phase flow within a calandria tube requires an educated solution.

The flow within the tube is buoyancy-driven and vertical [**10**]. Experiments using a circulation loop developed a theory which suggests that the ability of gas to transfer momentum to the liquid is debilitated as the rate of gas increases, which in turn lowers the circulation gain (Figure 3-6). Shorter tube lengths have long been known to be more efficient than those longer than one metre, as longer tubes mean that more vapour is present, which decreases the ability of the contents of the tube to conduct heat. .

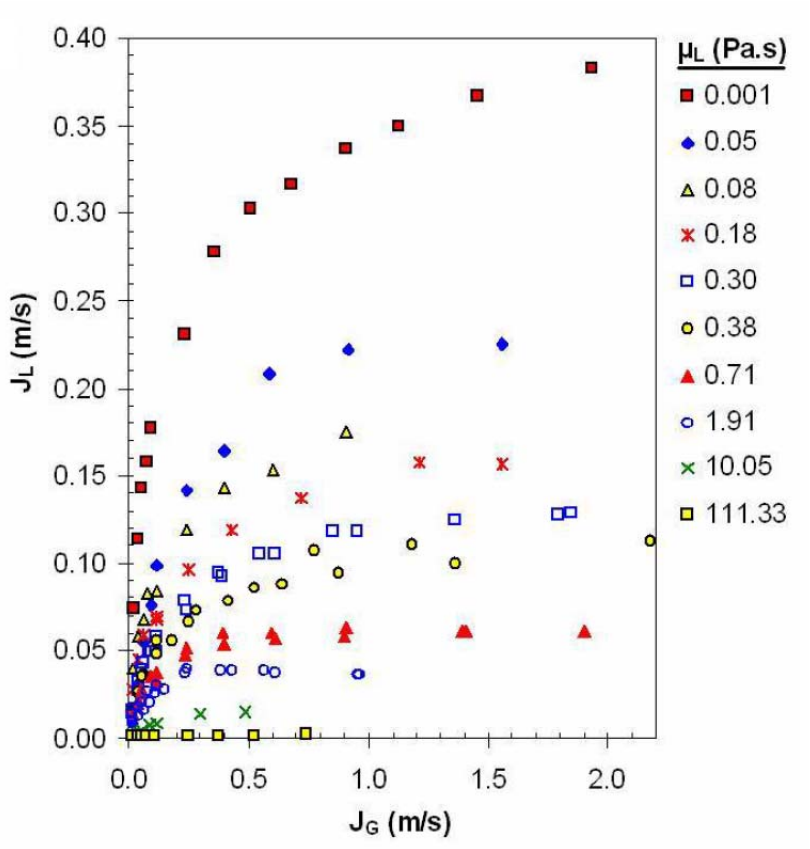

Figure 3-6: Circulation (J_L) within calandria tubes at different gas rates (J_G) and viscosities [10]

Figure 3-6 shows the circulation within a lab-scale single calandria test tube, with J_L representing liquid flux and J_G representing gas flux, where the phase flux is the result of the volumetric flow rate divided by the area of the tube, and is essentially an indication of the velocity of the massecuite within the tube. The fluxes measured at different viscosities μ_L (Pa.s).

Higher viscosities in the range of 0.7-110Pa.s present 'slug' behaviour where gas congregates into a single large bubble, with a pulsating circulation and strong vibrations. As viscosity decreases, the slug behaviour lessens, as does the vibration and severity of pulsating circulation.

With boiling, an increase in the frictional pressure drop occurs in the flow as the amount of gas in the tube rises. If the pressure drop in the tube increases, the slug formation becomes apparent. It therefore becomes necessary to reduce the drag on the flow as more momentum is dedicated to overcoming the friction, and less is transferred to circulation. Figure 3-7 shows the formation of slugs in the calandria tubes.

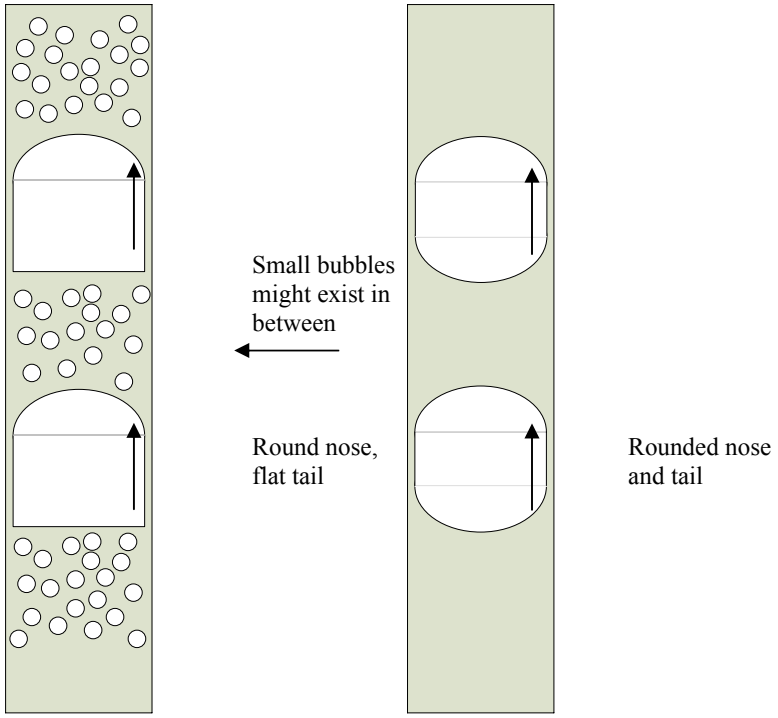

Figure 3-7: High viscosity (left) and low viscosity (right) of slug flow in pan tube [10**]**

If there is an abrupt change in viscosity resulting in the rapid formation of slugs in the heated tubes, the boiling could become unstable, which causes severe disruptions to circulation, pressure, temperature and evaporation within the pan [**11**]. Under certain conditions these conditions can become permanent, which could lead to intermittence in the flow process.

4. Implementation

There are several methods of implementing a tomographical system which have been discussed. This chapter concentrates on the implementation of the neighbourhood method.

4.1 Overview

A high-level overview of the system is as follows:

- Multiplex a bi-polar current injection into region of interest
- Demultiplex resulting voltages around region of interest into ADC
- Transmit data to PC
- Store data in appropriate form
- Apply reconstruction algorithm display image to user
- Append successive images into a video file

Due to the emphasis on data interpretation rather than speed or resolution, an online system where data is acquired and reconstructed in real-time is not of priority. The system needs to be sufficiently robust to endure the rigours of mill testing, and while electronics can be protected and housed with relatively minimal effort, the collars which are used to capture data do not afford that luxury, and considerable design effort went into their manufacturing.

4.2 Collars

The collars were the means with which data was collected from the pan. They were designed to create a ‘phantom’ above the top of the calandria tube in order to tomography the fluid dynamics immediately above the tube.

The collars were constructed out of PVC piping of diameter 100mm. Injection electrodes are made out of stainless steel squares, while sensing electrodes are merely bolt-heads affixed to the inside of the pipe.

When data (analogue or digital) is transmitted over a significant distance, the data-carrying wires need to be shielded. This is because electromagnetic interference can significantly alter the information being transmitted, especially when operating in a noisy environment such as a mill. When several data-carrying wires are grouped together the phenomenon cross-coupling can occur, where data present on one wire can electromagnetically couple itself onto a neighbouring wire. The longer the information has to travel, the worse these effects become. If the wire is wrapped in a grounded shield, the electromagnetic coupling and interference do not occur.

When testing a collar using unshielded wiring it was discovered that even when the collar was empty, a signal applied to one wire is present in some form on all the other electrodes; i.e. cross-talk is occurring which will corrupt data. This occurs when long data cables carrying analogue signals within close proximity to one another can electromagnetically induce currents on neighbouring wires.

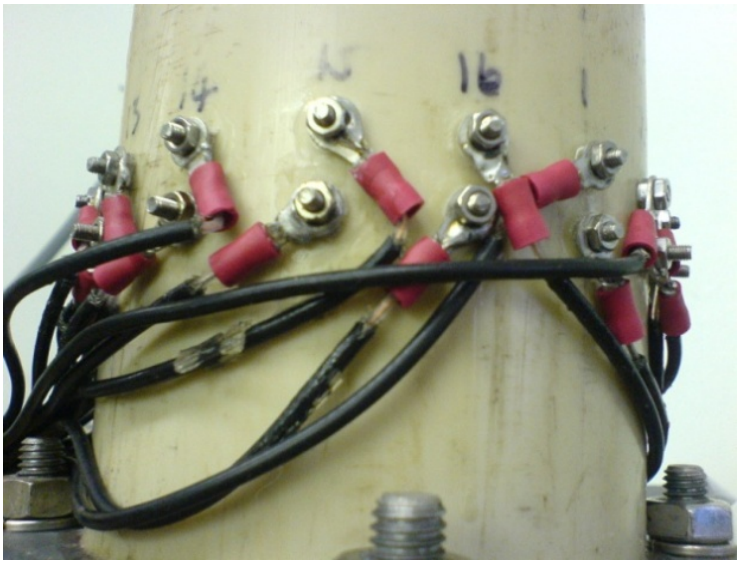

Figure 4-1: Co-axial cables connected to electrodes

In order to insulate and protect the electrical connections shown in Figure 4-1 from the volatile environment of the mill, the collars are coated in a fibreglass and resin mixture which provides

both strength and electrical insulation from the outside of the collar. Fibreglass is added to the mix as a resin-only mixture would crack in the heat of the mill.

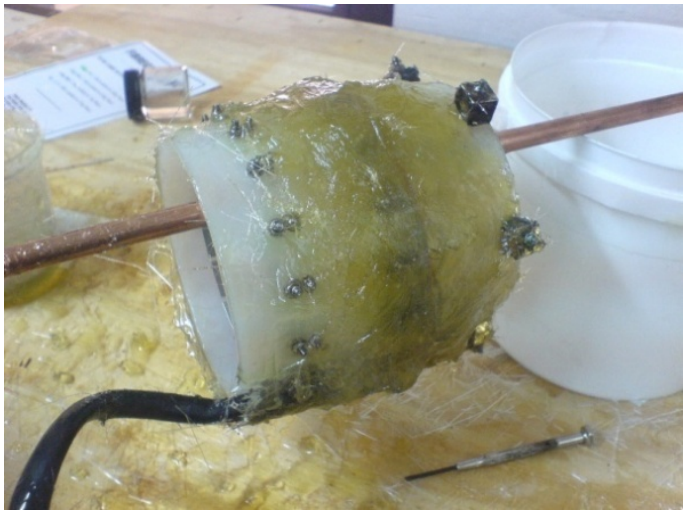

Figure 4-2: Collar midway through resin coating process

During a sugar ‘strike’, the entire mass of sugar/massecuite (approximately 50 tons) is released through in a very short time. This results in a large suction force pulling anything within the pan towards the centre of the floor (the ‘down-take’), hence the collars need to be fixed to the floor very securely. If the collars come loose, they get severely damaged during each strike.

The first method used 6*12mm square rare-earth magnets to hold the collars down. These were drilled through the centre and bolted to the sidewall of the collars, as shown in Figure 4-3. The first generation of collars had the cabling protruding from the top of the collar as seen in Figure 4-2, however during a strike there is a torque moment applied to the top of the collar, increasing the probability that it could become loose, therefore in future designs the cabling was modified to protrude from the bottom of the collar.

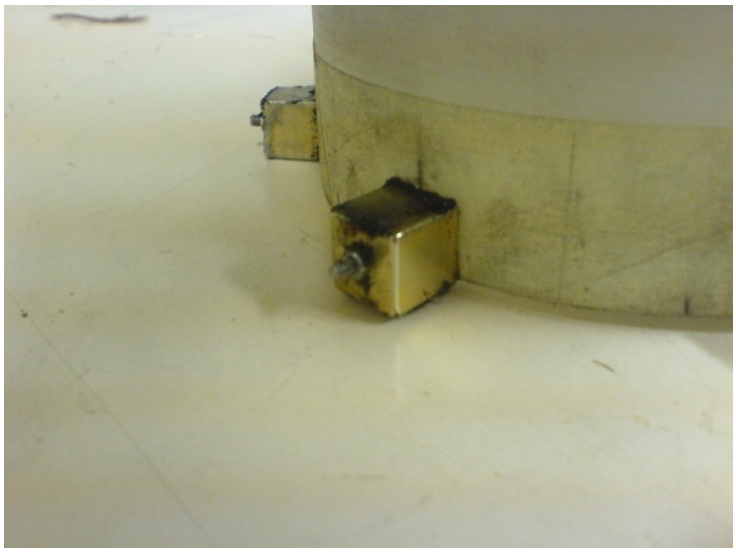

Figure 4-3: Rare-earth magnets attached to base of collar

Once placed in a pan, however, the cabling connecting the collar to the wall is still free to move about within the pan. Attempts to minimise this effect did not prove successful, and hence the forces acting on the collar and magnet were still sometimes strong enough to either dislodge the magnets completely, or as is more common and after a number of successive strikes, pull the bolt-head through the PVC and resin! To rectify this, three further designs were tested:

- An L-shaped bracket bolted to the side of the collar with the magnet attached underneath. A prototype of this design was tested during a data capturing event, however the collar had disappeared after one strike (see Figure 4-4 (a) below).
- A circular steel ring bolted to the outside of the collar base, with the magnets bolted to the ring (see Figure 4-4 (b) below).
- A magnet-less design, where an L-shaped bracket is bolted to the pan floor by welding a bolt head to the floor. This proved to be the most successful method (Figure 4-5).

Figure 4-4: (a) L-shaped bracket and (b) steel putty encasing magnet and circular steel ring bolted to collar with magnet attached on outside

Figure 4-5: Final collar attachment design

After several attempts at data capturing in the mill failed due to collar detachment using the magnet design, a triangular jig was used which would allow accurate placement of holes drilled into L-shaped brackets (Figure 4-5 and Figure 4-6). Using this test jig, bolts were then welded to the floor of the pan (Figure 4-7 (a)), and the collar was slid over the bolts and secured - to solve the problem of cable drag during a strike, nuts were welded to the floor of the chamber in a vertical fashion (Figure 4-7 (b)), and cable ties were used to secure the cables in place. This final method proved successful, and the collars and cables were still in place and intact after several days (and numerous strikes) in the pan.

Figure 4-6: (a) Final collar design with jig attached and (b) jig in position over tube prior to welding of bolts

Figure 4-7: (a) Bolt for collar and (b) nut for cable

Figure 4-8 shows how three collars were laid out within the pan for the final test. The collars were laid out in a radial line from the wall to the centre of the pan, next to the down-take. This was because the steam that heats the tubes beneath the tube floor is injected at the wall of the pan and flows inwards towards the drop. A radial measurement might provide insight as to how the centre of the pan compares to the edge of the pan in boiling terms.

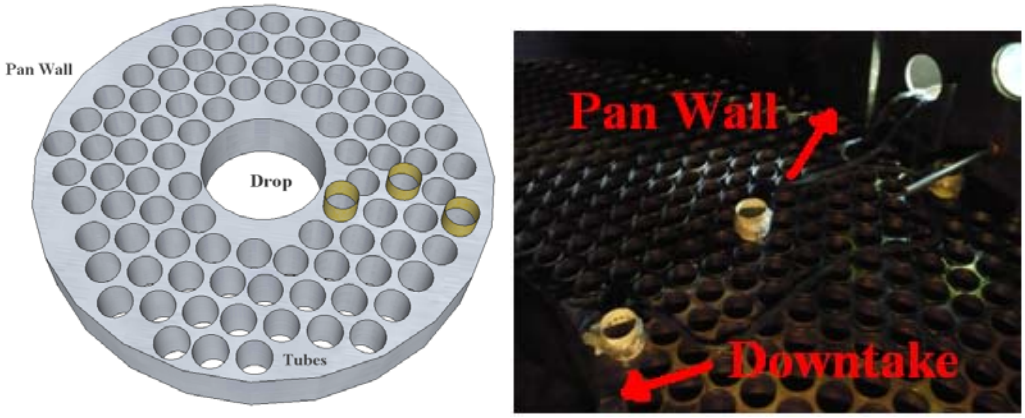

Figure 4-8: Layout of collars within vacuum pan (sketch not to scale)

In order to send data back from the collars to the electronic hardware, the cable is required to pass through a porthole in the pan wall which is normally used to view massecuite levels within the pan. As mentioned an iron plate was constructed to replace the existing porthole, and drilled to enable the cable to be passed through, as seen in Figure 4-9.

Figure 4-9: Iron plate

4.3 Electronic Hardware

The electronics of the system is based around the ATMega162 microcontroller and DaqBook 2001 Data Acquisition board. Together these devices control the current injection and voltage measurement, and send the data packets to a PC. The electronics were designed to be modular, so that a greater number of collars and hence sensing zones could be added to the system at will, in a plug and play fashion.

4.3.1 Electronics Overview

It is desirable to have minimal contact resistance between an electrode and the medium which is being studied; therefore a signal source with a high output resistance is required. A Constant Current Source (CCS) has characteristically high output impedance, and hence is the logical choice for tomography applications [**12**], [**13**], [**4**][**14**].

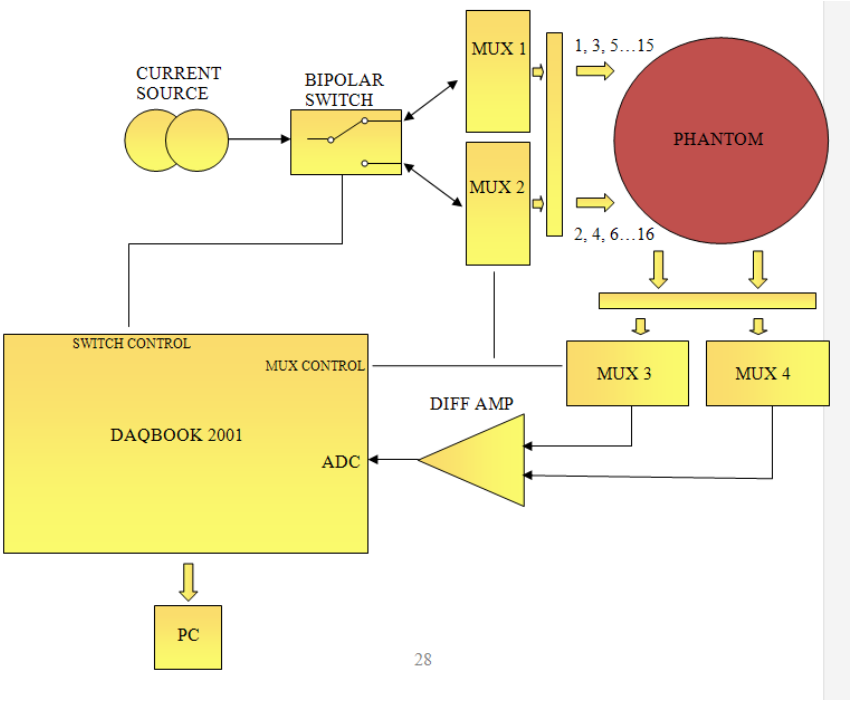

Figure 4-10: Electronics overview

Figure 4-10 shows an overview of the electronics governing system control. A CCS delivering a constant Direct Current (DC) feeds into a switch which converts the signal into Alternating Current (AC). The AC signal is multiplexed through to the individual electrodes. The return path signal is multiplexed in a similar manner and connects to a differential amplifier which outputs to the ADC stage.

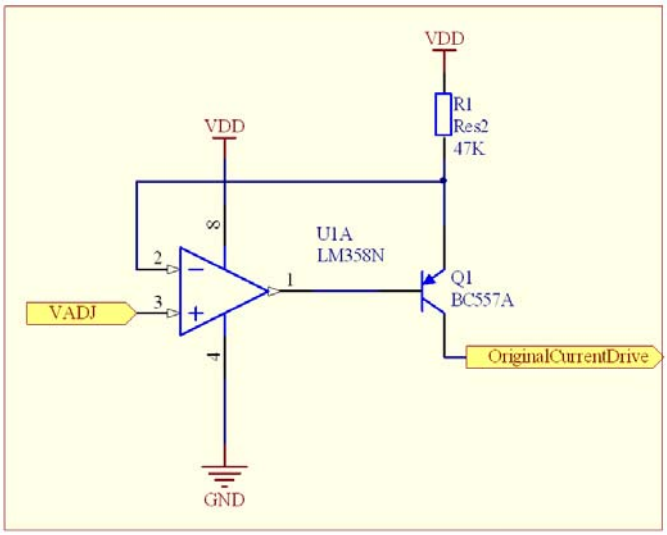

Figure 4-11: Constant Current Source

Figure 4-11 shows the current source used in the system. On the premise that $V_+ = V_-$, the voltage on Pin 3 of the LM358 is set using an external potentiometer, therefore also setting the current flowing through the 47kΩ resistor as seen in Figure 4-11. If the pnp BC557 transistor is operating in saturation mode, $I_C = I_E$, hence if I_C is held constant so will I_E, regardless of the resistance in the emitter path, provided the required current through the load does not require a voltage source greater than the supply voltage.

4.3.2 Bi-polar switching and multiplexing

If a current is induced between two electrodes, electrochemical effects (reduction and oxidation) can influence the flow of electrons through the ions of the medium. This effect can be negated by applying an alternating current waveform to the electrodes, such that the anode and cathode of the electrode pair is constantly switching, reducing the amount of oxidation and reduction occurring. A bi-polar DC pulse is easily implemented to achieve this. Modulation and demodulation circuits can also achieve the same result, however they are much more complex to implement, and they are also limited in terms of frequency of operation. A higher switching frequency means that more tomographical images per second can be obtained.

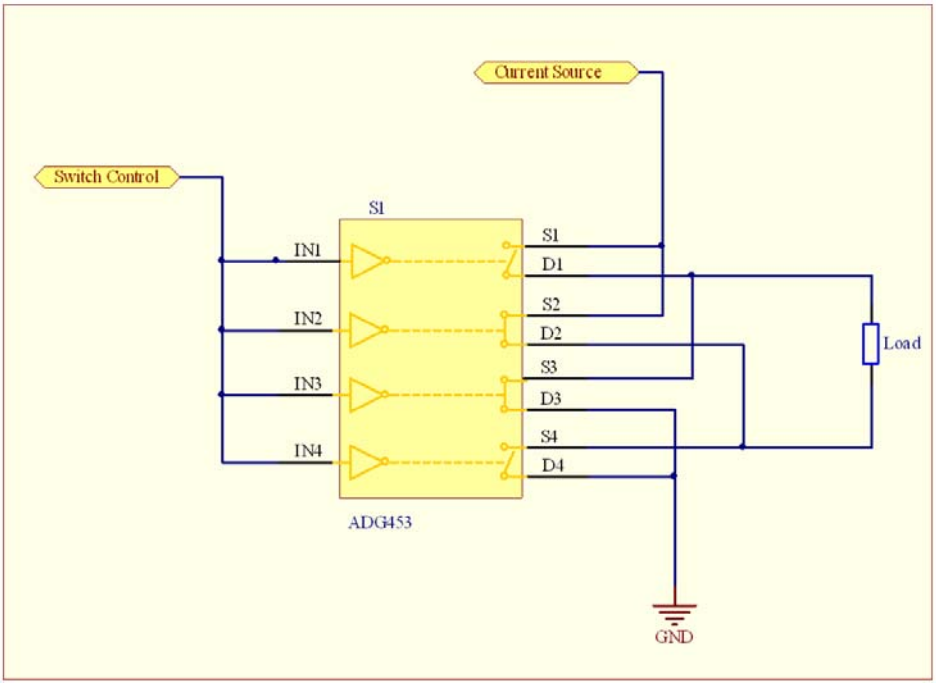

Figure 4-12: Bi-polar switch configuration

The ADG453 is a chip which contains 4 independently controlled switches, however in this application they are wired to serve as an H-bridge in order to provide the alternating current waveform required. The On channel resistance is 40Ω, and each switch can sustain 100mA. A control signal from the DAQBOOK which is common to all the switch control pins sets up the bi-polar current injection through the load, in this case the medium which is being studied.

The current from the switch is then multiplexed to the sixteen different electrodes. The multiplexers are wired up so that current can flow in either direction to and from the current source. Multiplexer A1 serves the odd numbered electrodes, and Multiplexer A2 serves the even numbers, as shown in Figure 4-13.

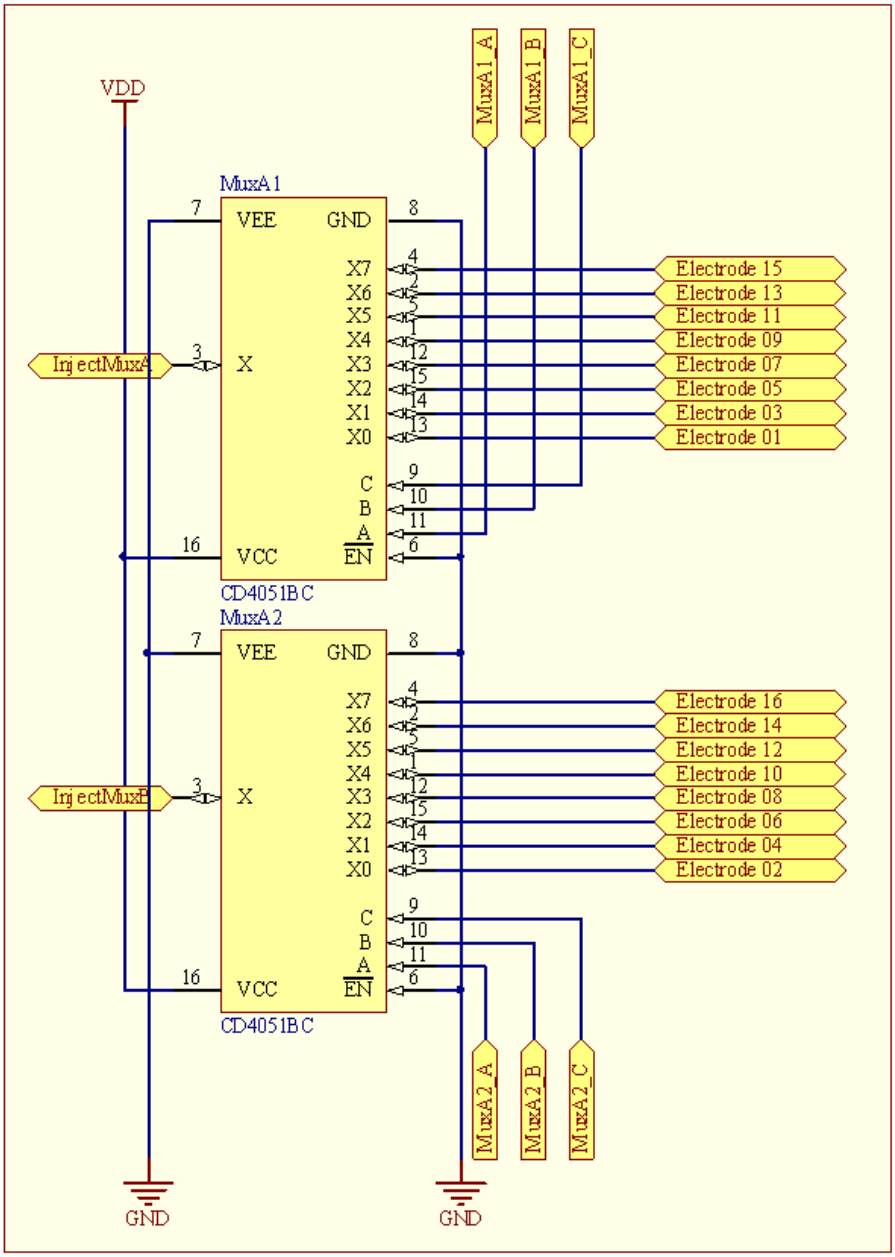

Figure 4-13: Injection Multiplexing circuitry

The multiplexers are required to route signals up to 15V in magnitude, and require control signals that are equivalent to the power supply. Normal TTL-level control signals therefore are not sufficient to control the multiplexer, and hence a level translation circuit is required, operating on the 'active-low' principle, shown in Figure 4-14.

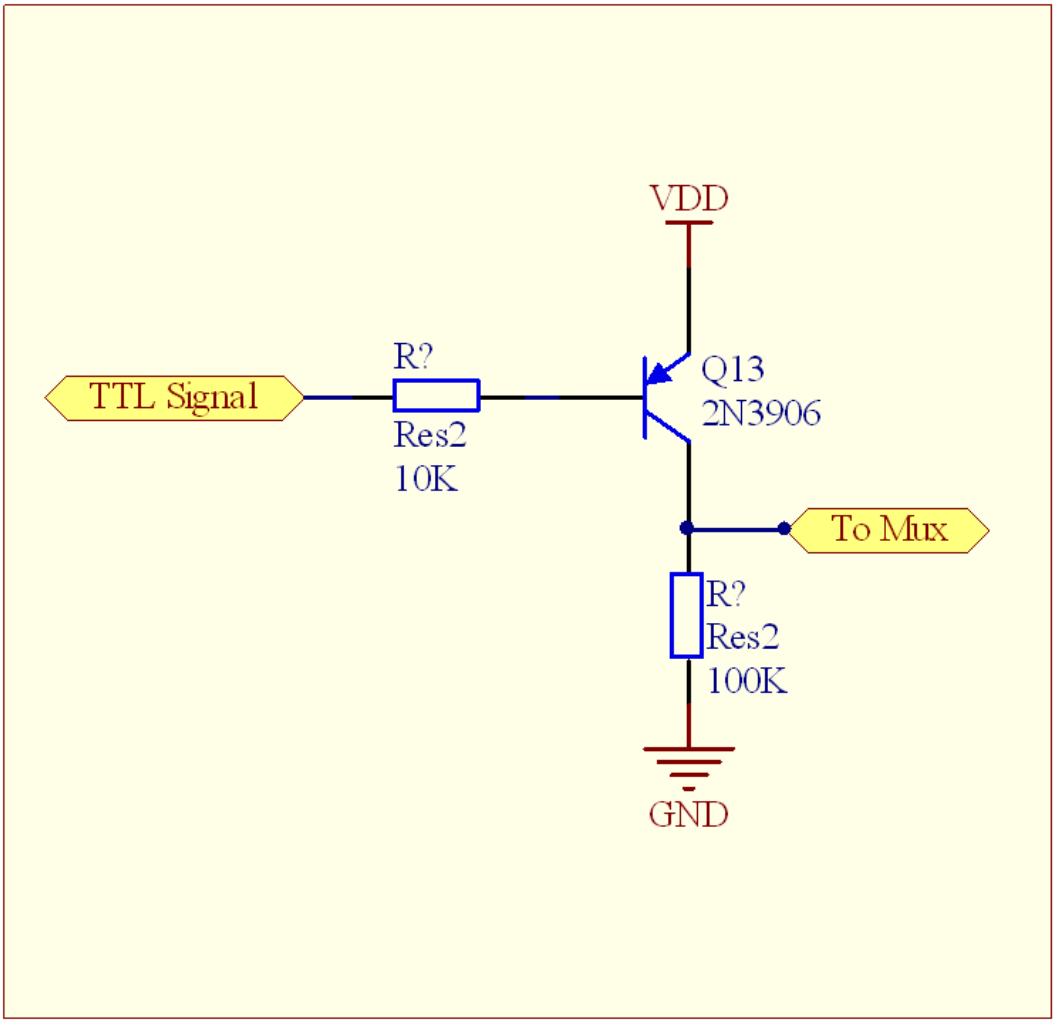

Figure 4-14: Level translator

In a similar manner to the current injection, the voltage sensing is routed through two multiplexers, one serving odd numbers and the other serving even numbers. The result is a differential voltage between the two electrodes which are routed through the multiplexer, before being differentially amplified and passed on to the ADC. The differential amplifier is shown in Figure 4-15.

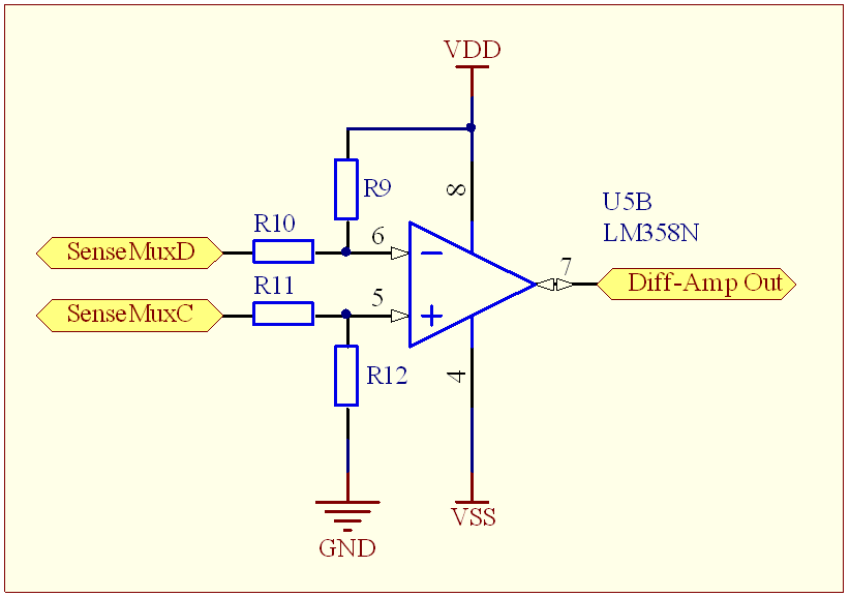

Figure 4-15: Differential Amplifier configuration

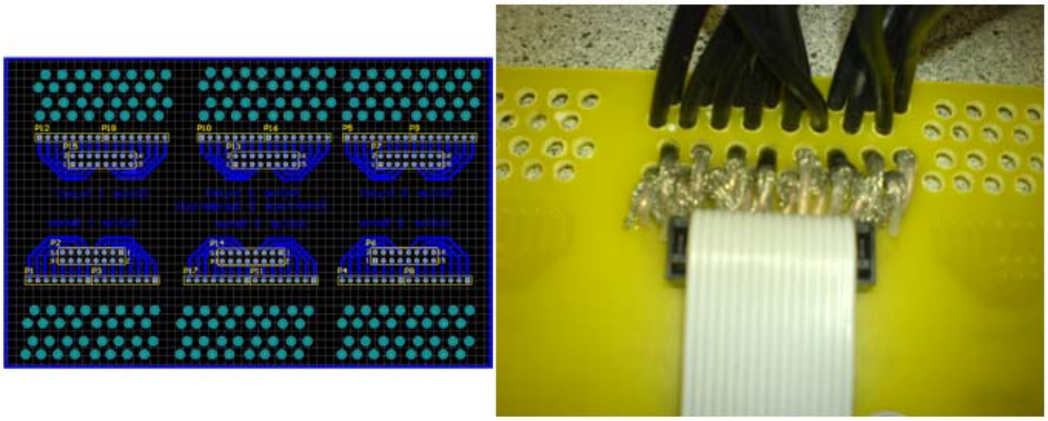

Figure 4-16: Connector board for collar wiring

The collars connect to the electronics via a connector board as shown in Figure 4-16. The co-axial cable is threaded through two holes for mechanical stability, and a boxed header ribbon cable feeds the relevant signals to the control boards.

4.3.3 Control

The control of the system is managed at a macro level by the DAQBOOK 2001 and at a micro level by the ATMega162. The DAQBOOK is integrated to the DASYLAB software package. It can perform analogue sampling at 400 kHz on 8 differential or 16 single-ended channels.

DASYLAB, the DAQBOOK 2001 and the ATMega162 are all connected via digital I/O lines. User interface is handled by DASYLAB, the main control being a ready pin which puts the microcontroller in standby mode. The microcontroller handles the incremental algorithm which determines which electrode pair is currently configured as the current injectors, and which electrode pair is currently being read from, as well as controlling the bi-directional switch. The microcontroller also controls the ADC sample triggering.

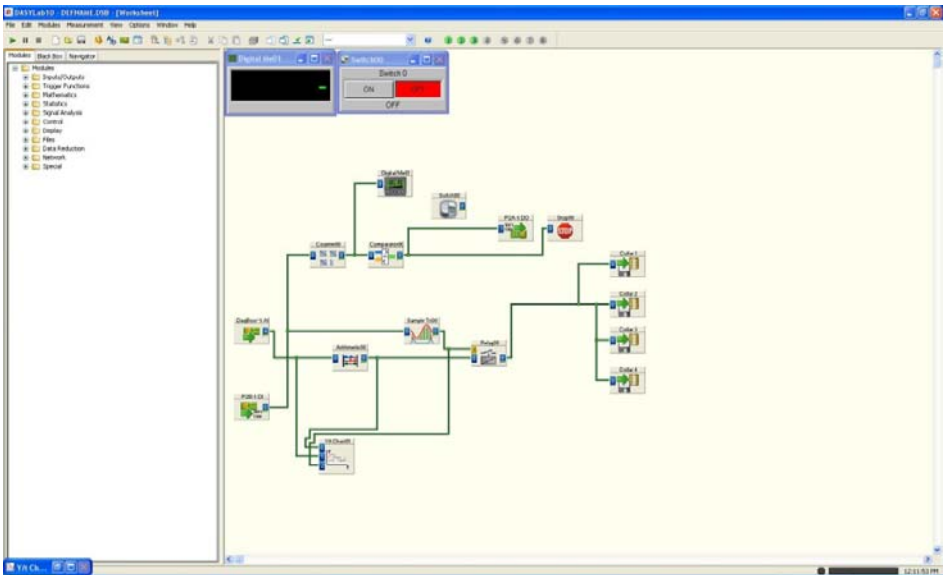

Figure 4-17: User interface in DASYLAB

The current source is continuously active; therefore a means of removing it from the signal path is required for when the system is on standby. A SPST solid state relay suffices for this.

For each data point of the 208 values obtained, four measurements are taken, two in the positive half of the cycle and two in the negative half. In software these values are averaged to provide a single data point. The read timing of the ADC is controlled by a strobe signal generated by the microcontroller. The period of the strobes are set to 25% and 75% of the total switch period, respectively.

4.3.4. PCB Design

The Printed Circuit Boards (PCBs) were designed using the Altium design package, an offshoot of Protel and are shown in Appendix 1. A single control board is used to control up to eight collar interface boards (this number is dependent on the number of ADC sampling channels available at the data acquisition module) and houses the power supply and microcontroller, together with the logic level translator circuit, shown in Figure 4-18 and Figure 4-19.

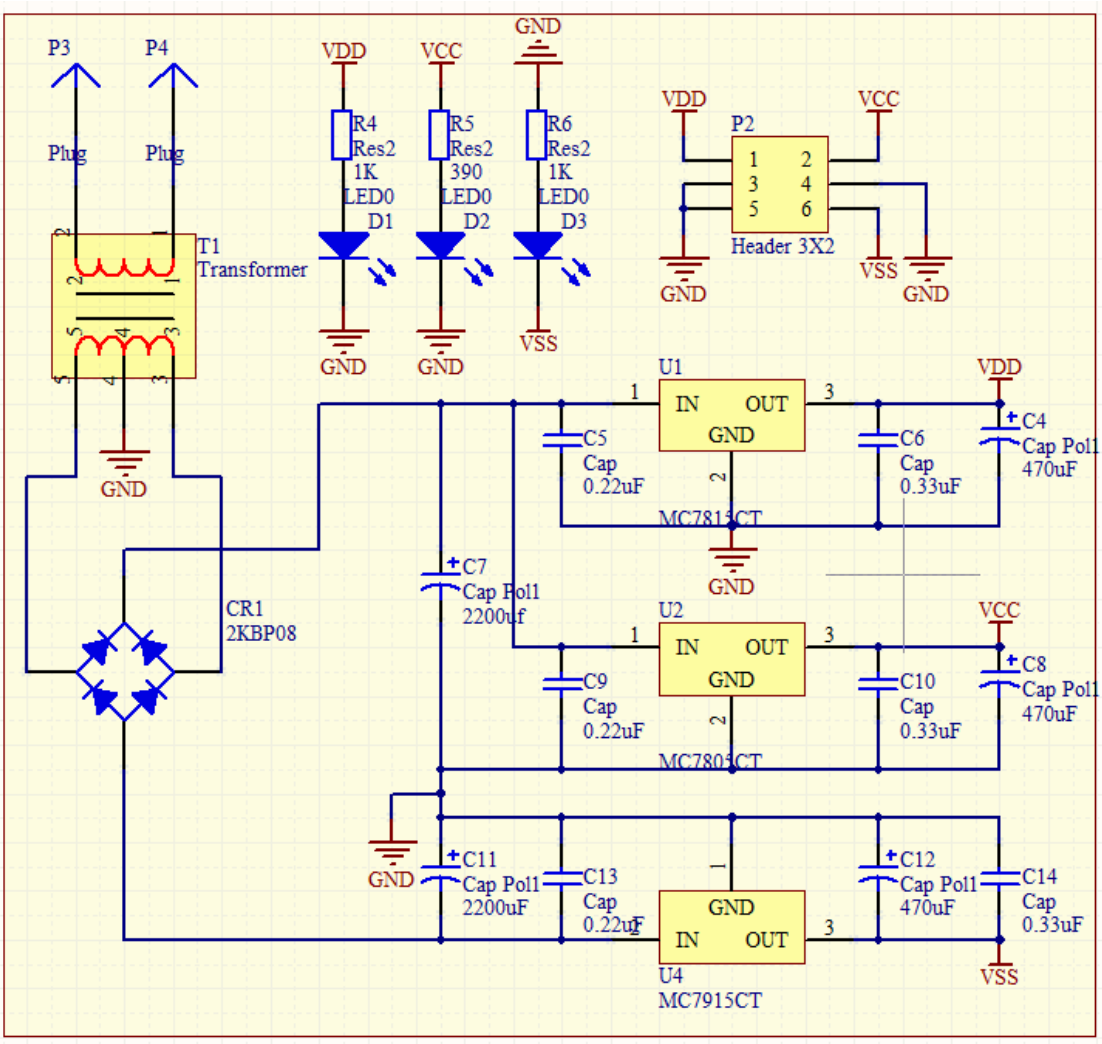

Figure 4-18: Power supply for tomographical system.

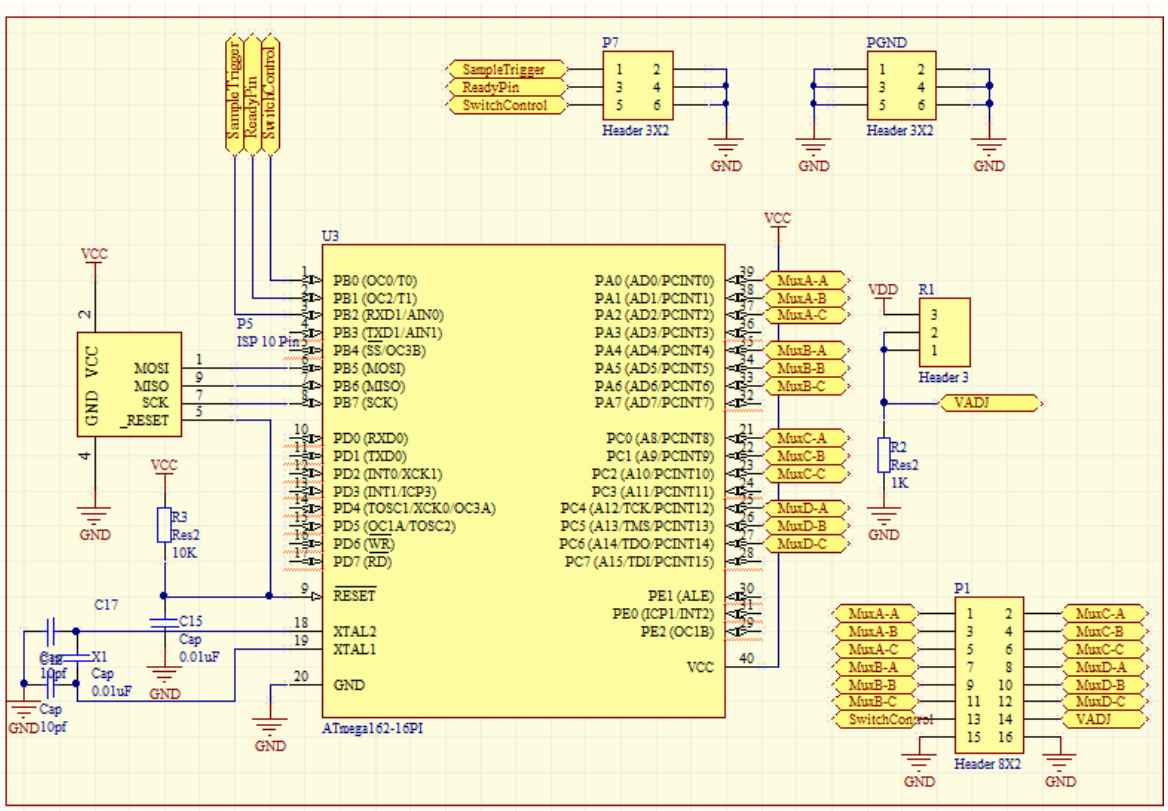

Figure 4-19: Modularised Control Module

Three power levels (5V, +15V and -15V) are generated on the control board and are paralleled to the daughter boards via ribbon cable, as are the various control signals.

The interface boards contain the CCS, relay, bi-directional switch, multiplexers and differential amplifier and are named “MuxMe”. These boards are the modular components of the tomography system; each one controls a single phantom, and because of the parallel nature of the control signals and power supply, any number of phantoms can be implemented as long as there are sufficient ADC sampling channels available.

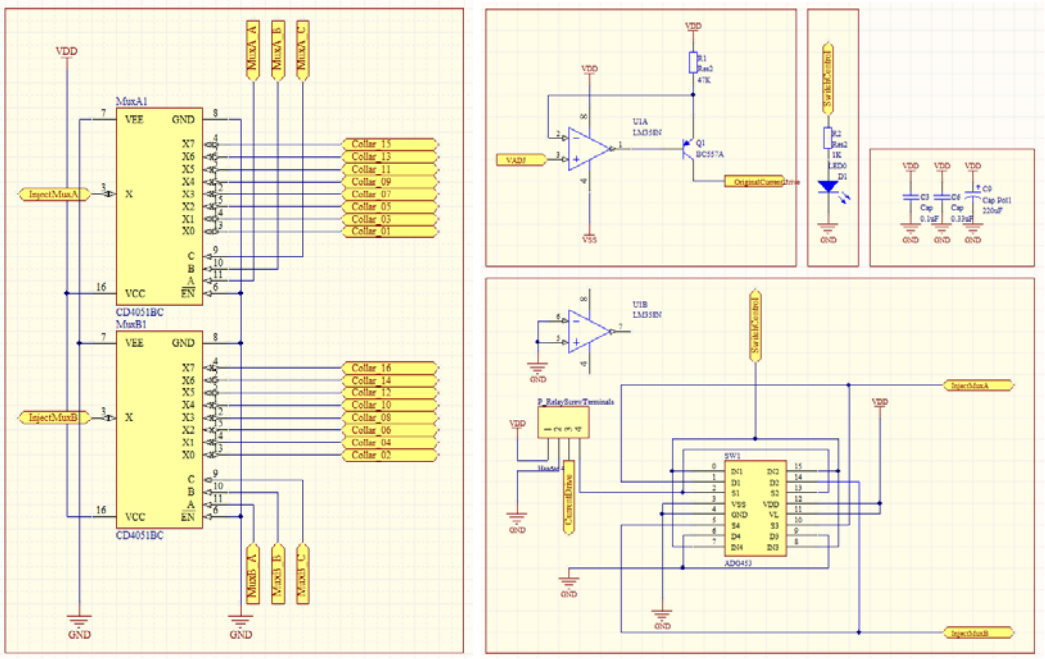

Figure 4-20: Modular MuxMe Schematic showing current source, bipolar switch and multiplexers.

4.4 Image Computation

The image reconstruction software was developed in MATLAB, which is an excellent prototyping, development and analysis tool. To create a tomographical image, the measured data set from the DaqBook must be converted into the correct matrix form, compared to a reference data set via an algorithm, and depict the end result from which individual pixel values are generated.

As discussed in Chapter 2, the image reconstruction technique back-projects the change in measured voltage conditions at the periphery of the phantom to the conductivity values of the ‘resistance zone’ which is encompassed by the equipotential lines terminating on the measuring electrodes, shown in Figure 4-21, where resistance has been introduced between electrodes 4

and 5. The weighted difference between measured and reference voltages is greater than that of the other resistance zones [**2**], [**15**], [**16**].

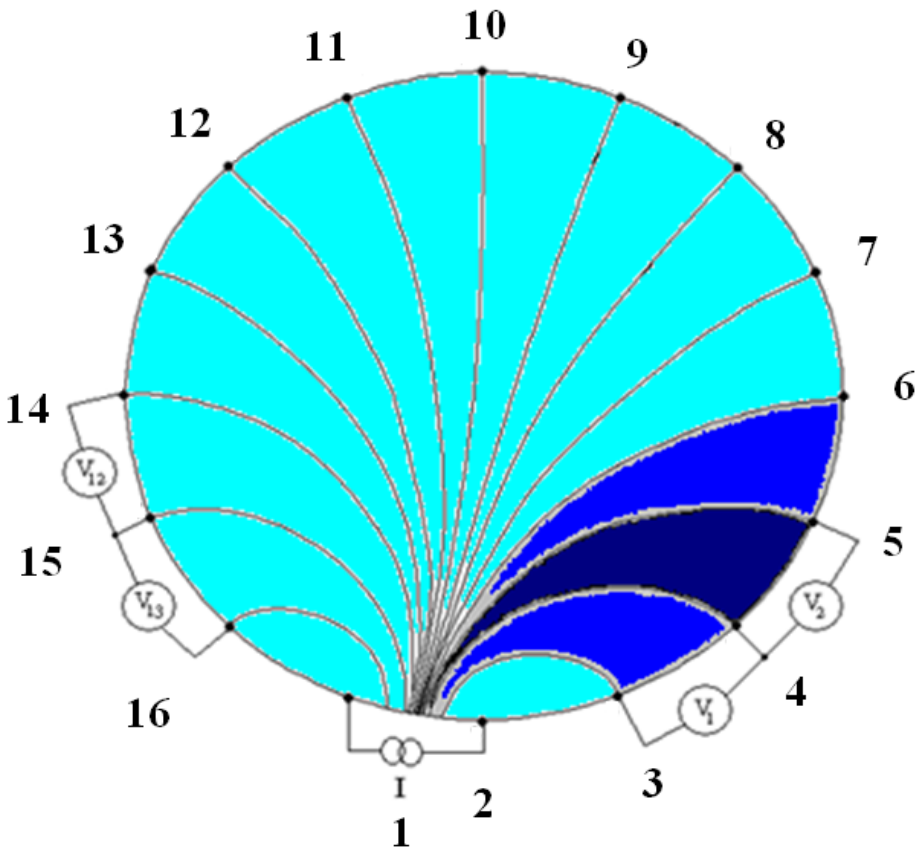

Figure 4-21: Equi-potential lines within phantom

Each neighbouring boundary measurement taken is related to the expected boundary measurement under homogeneous resistance conditions. This determines the difference between expected and measured values for the resistance zone that the neighbouring electrode equipotential lines encompass. This process is repeated from each injection electrode pair and the final image is a super positioned compilation of each weighted slice as according to the Newton-Raphson method. The flow diagram of this process is shown in Figure 2-2.

The neighbouring boundary measurements are related to the expected boundary measurements which would occur under homogenous conductivity conditions, which determines the amount of change within the resistance zone bounded by the equipotential lines. This process is performed

on each injection electrode pair and each successive result is super positioned for each weighted slice to produce the final image.

Matlab's Partial Differential Equation Toolbox ™ (PDE Tool) was utilised in order to determine the co-ordinates of the resistance zone affected by a conductivity change as in Figure 4-21. PDE Tool allows the definition of a partial differential equation problem to be stated by the creation of a 2-dimensional object (such as the regions of the tomographical phantom) with specific boundary conditions.

The boundary of the phantom is defined as a circle of radius 0.8. 16 electrodes of radius 0.03 represent current injection and sinking and voltage measurement.

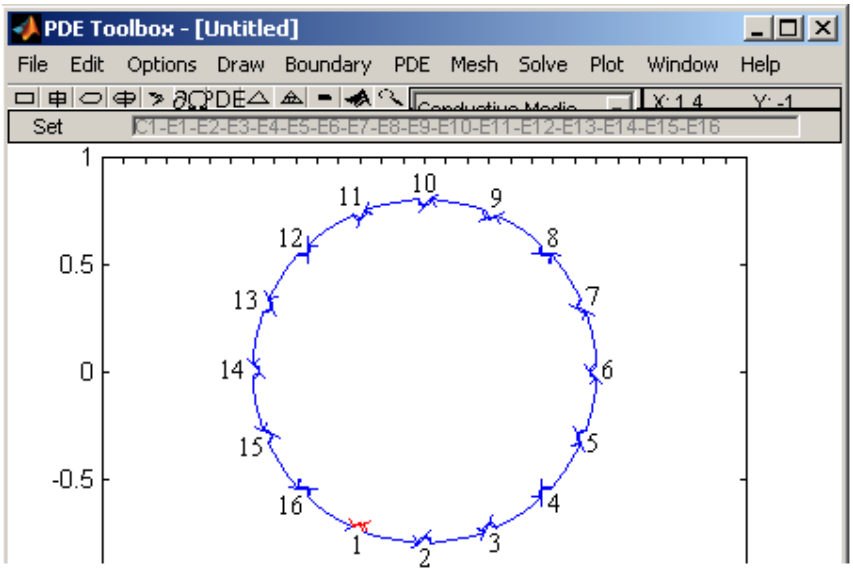

Figure 4-22: 2-dimensional cross-section of phantom in the PDE Toolbox

The PDE Toolbox can then apply a mesh to the problem so that the approximation of the solution can be determined.

The structure of the mesh can be of any number of nodes initially, as the simulated boundary conditions data only needs to be run once, and can be stored for further experiments.

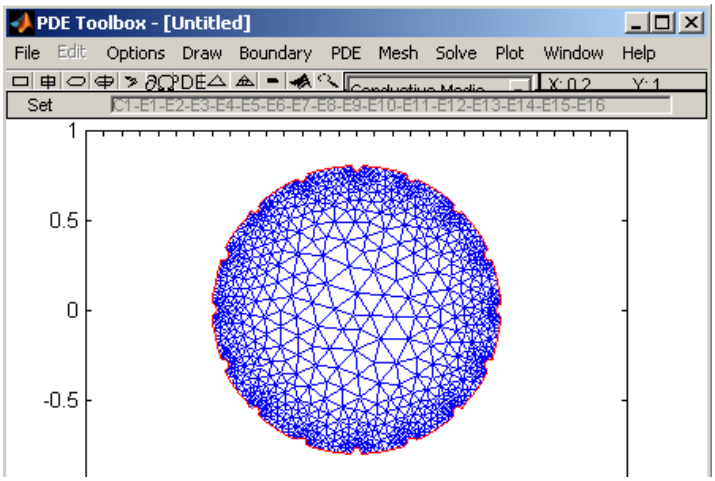

Figure 4-23: Initial mesh structure over which the simulation PDE solution will be applied

Finally, the PDE Tool visualizes the results over the mesh.

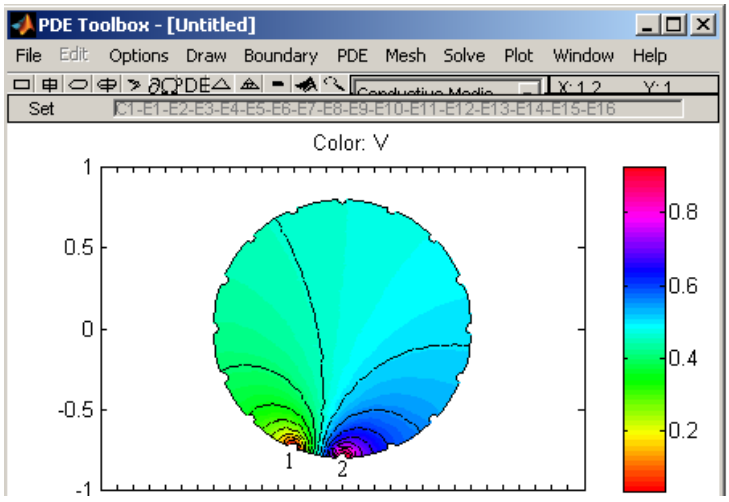

Figure 4-24: Simulated partial differential solution with current injection on electrode 2 and current sinking on electrode 1

The resistance zones of the phantom need to be determined empirically and so the boundary conditions for the simulated data set are:

$$V = V_0 \tag{4.1}$$

and

$$\rho^{-1}\frac{\delta V}{\delta n} = J_0 \tag{4.2}$$

where ρ and V are the conductivity and voltage distributions within the 2-dimensional model, and V_0 and J_0 are the boundary voltage and current densities, and n is the electrode injection number. For simulation, ρ was assumed to be 1Ω.

The boundary conditions in Figure 4-24 are set up in the PDE Tool by applying 0V to Electrode 1 and $\delta V/\delta n$ = simulated current flowing through Electrode 2. The remaining electrodes are set to $\delta V/\delta n = 0$, meaning that the remaining electrodes act as high impedance boundaries through which no current can flow.

5. Results

This chapter discusses the performance of the system with two core objectives in mind; firstly, can it detect a range of resistive regions, and secondly, does it give an accurate representation of the boiling characteristics within a given tube?

Laboratory tests were performed on a prototype test rig, which allowed refinement of the mill hardware. Due to the unavailability of massecuite in a lab environment, de-ionized water was used in its place. The water was then mixed with saline until its conductivity equalled that of massecuite under boiling conditions.

The final frame rate of 7 captured Tomographs per second is converted into a video file (*.avi). Each captured image is appended into the file which is set to playback at 7fps, presenting an actual speed video to the user. The frame rate was set as such by the medium – more captures simply were not possible (discussed in Chapter 3).

The video returned to the user is a graphical representation of the cross-sectional spatial conductivity within the phantom. High conductivity (low resistivity) is denoted by dark blue, and low conductivity values (high resistivity) values assigned to dark red, with a linear scale separating the two, where values are normalized. Figure 5-1 shows a sample frame of raw data with an empty phantom. Clearly visible are the equi-potential electric field lines branching out from the electrodes.

5.1 Laboratory Results

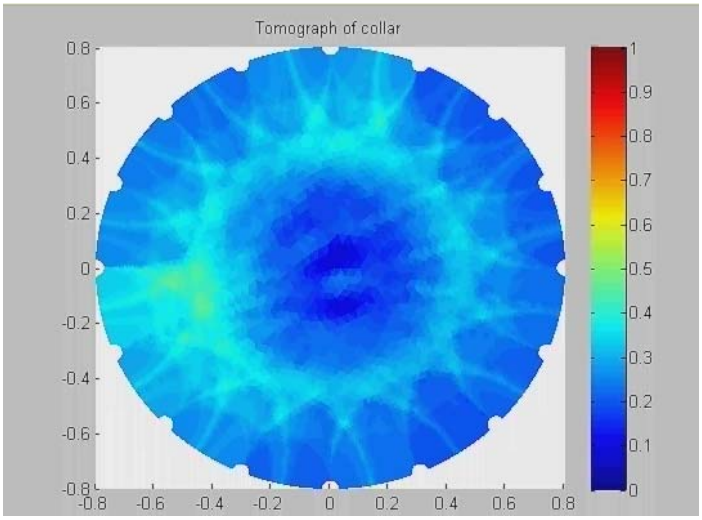

Figure 5-1: Sample frame of raw data, phantom containing homogeneous medium

Figure 5-2 shows a raw data frame where a ping-pong ball (simulating a bubble) is inserted into the tomography layer. The region of high resistivity produced by the artefact is clearly apparent as the red area in the upper left quadrant of the phantom.

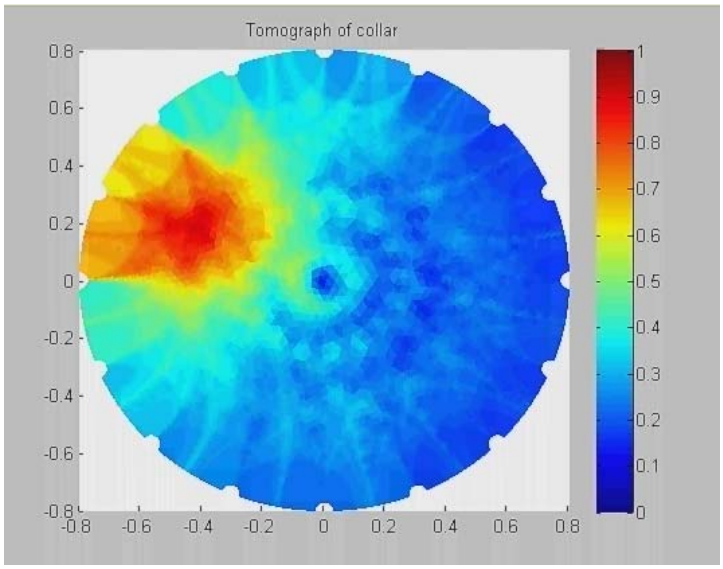

Figure 5-2: Raw data, high-resistance area in top left quadrant

tomographical images can be filtered for clarity, with the normalized values following a quantisation scheme of:

- 0 – 0.3 becomes 0
- 0.3 – 0.5 becomes 0.4
- 0.5 – 0.7 becomes 0.6
- 0.7 – 1 becomes 1

Quantizing the videos in this manner greatly aids in clarity when detecting bubbles (primary aim of project). Figure 5-3 shows a frame of a video which was a laboratory experiment where air was blown through the prototype collar. Bubble formation is clearly visible in the Tomogram.

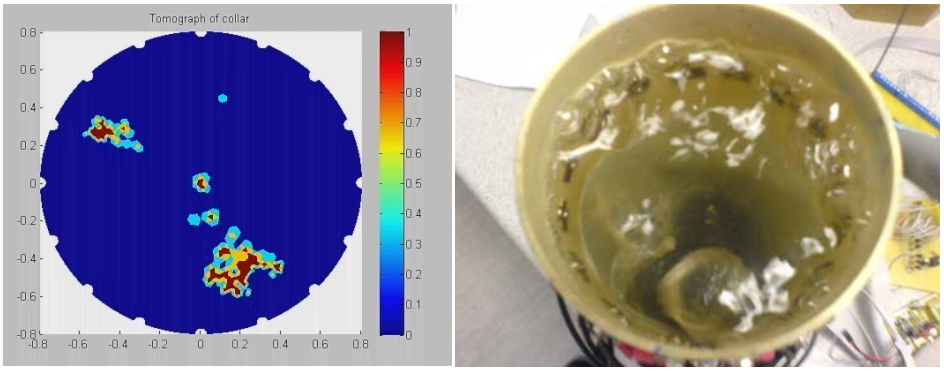

Figure 5-3: Quantized data showing bubbles

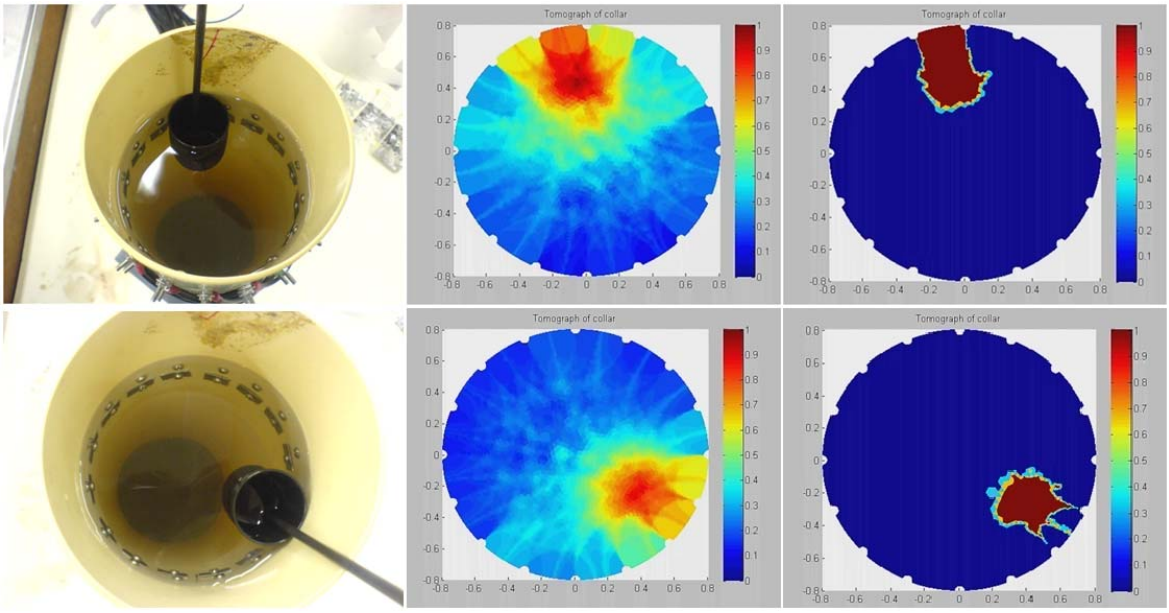

Figure 5-4: Real, raw and filtered tomographical images

Figure 5-4 shows some examples of data captured in the laboratory using the scale calandria tube model. Deionised water which was calibrated to the same resistance as massecuite was used as the medium within the phantom.

5.2 Mill Results

Access to a sugar mill is a tricky business as the mill runs continuously – any down-time results in a massive loss of revenue for the company. Individual pans are run 6.5 days of the week and are only shut down for a few hours for maintenance every week. These individual down-times are overlapped amongst the pans so that the mill is always in production. Gaining access to the pan was not always convenient for the mill and hence it was a privilege to be allowed to take measurements.

This chapter presents two contrasting mill experiments, where different boiling dynamics are presented. Testing was done at the Maidstone sugar mill, near Tongaat in KwaZulu Natal. Successful results were obtained on 17th August 2008, 23rd November 2008, and 20th October 2009.

5.2.1 August 2008

In August of 2008 the first successful measurements were taken in the pan, using a prototype system with only one collar. The aim of this experiment was to confirm that the system could detect the different boiling stages within the pan environment, as well as collar stability during boiling and a strike. Data capturing at this point was performed at 5 frames s^{-1}. Measurements were taken during the following activities:

- Steaming the pan prior to being filled with massecuite
- Initial syrup + steam run (creates a foamy mixture)
- Pan full of massecuite prior to boiling
- Pan 40% full , 61°C, -89.6kPa

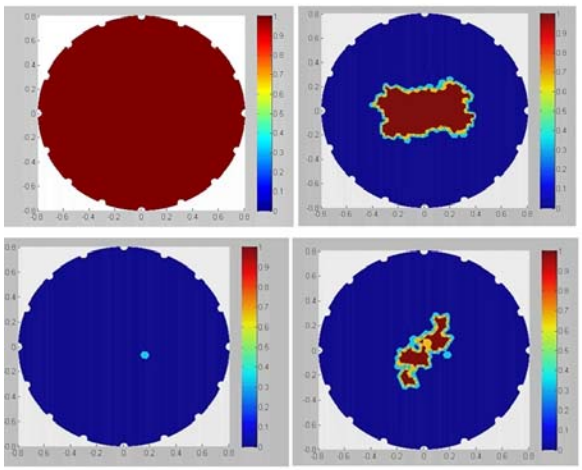

Figure 5-5: Steaming pan (a), pre-boil foam (b), inactive (c) and boiling (d)

This experiment was performed using the original collar attachment design (rare earth magnets). A week after the readings were taken the collars were still in place, confirming that the data received during the experiment depicted flow of massecuite and bubbles through the top of the tube, as opposed to random massecuite movement had the collar been knocked out of place – as was the case with all future attempts which used the magnet design when attempting to introduce multiple collars into the pan.

As seen in Figure 5-5; empty, full inactive, foaming and boiling stages were all detected as expected. The foam stage is pre-boil, where the pan is prepared for the creation of massecuite. Pressure is dropped to the -80kPa range and temperature is lifted to around 60-70º C. The 'mother liquid' present at this point to help seed the crystal growth in the boiling stage begins to form a foam until temperature and pressure are stabilized. As it is not possible to obtain 'ground-truth' images as a reference in the pan, the expectations of the expert pan boilers was used as ground truth.

5.2.3 November 2008

In November 2008 several expeditions to the mill were undertaken. The prototype system using one collar which was employed in August was expanded and upgraded to include three different collars. One collar was fitted with a double row of sensor zones in order to determine if the velocity of bubbles could be ascertained (see Figure 5-6).

Figure 5-6: Double-layer collar about to be installed in pan

Due to the initial success of the experiments in August of that year using the rare earth magnet attachment technique, the same method was used for these experiments. However, despite considerable effort to ensure that the magnets were attached as accurately and strongly as possible, the technique failed to keep the collars affixed to the pan floor during a strike - making data capture somewhat difficult. After seven returns to the mill and numerous collar redesigns, one set of collars remained stationary for the duration of a strike during which suitable data was obtained.

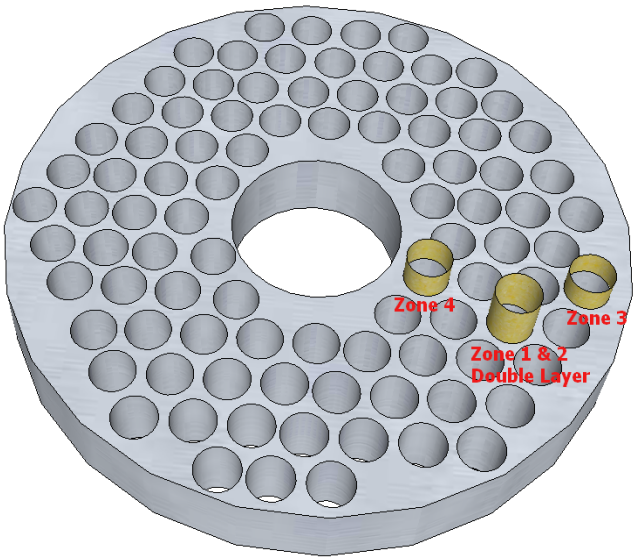

Figure 5-7: Layout of collars within pan for second test – Zones 1 and 2 form a double collar

The collars were positioned within the pan such that measurements could be taken near the pan wall, midway to the downtake, and next to the downtake. The numbering of the sensor zones was as follows:

1 – Double collar bottom

2 – Double collar top

3 – Single collar near pan wall

4 – Single collar near downtake

The results from this test differed substantially from those of the August test. The August results showed a distinct difference between foam and boiling, with the boiling in particular forming 'bubbles' which grew and shrank in a manner expected. The foam section of the August test was not repeated in November, as the pre-boil foam is not always formed before a boil and is dependant on the nature of the massecuite of that particular day. The November test which eventually produced useable data depicted inactive and empty sensor zones as expected; however during periods of activity instead of a 'bubbling' formation there appeared a single continuous area of high resistance in the centre of all four phantoms. The only indication of boiling was in the size of this area of resistance, which initially was relatively small and grew in time before stabilising.

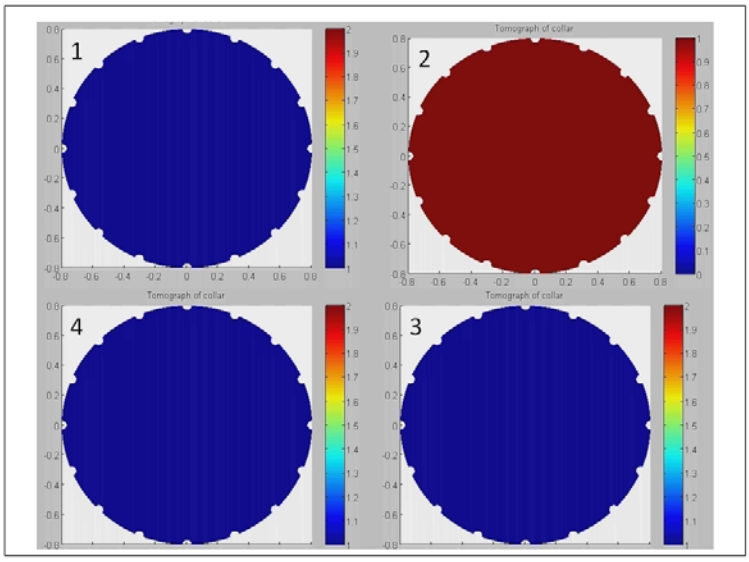

Figure 5-8: Pan beginning to fill in Zones 1 through 4

Figure 5-8 shows the first reading as the pan was fed with 'mother liquid' – a small amount of massecuite from a previous batch which is normally used to seed crystal growth. As can be seen, the sensor zones close to the pan floor all show a homogeneous result with the top zone (Zone 2) of the double collar showing an empty phantom. Average vapours vs. liquid percentages were calculated for each reading as they did not vary much over each reading.

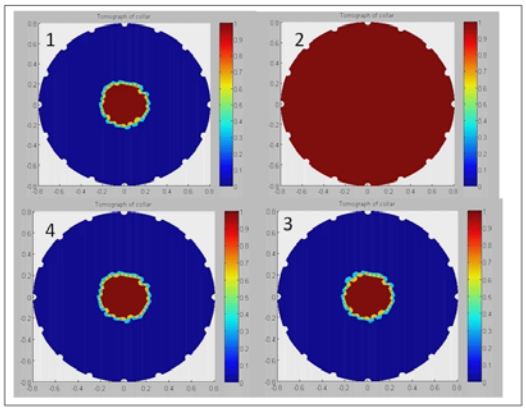

1 – Double bottom

Vapour vs. Liquid: 7.4%

2 – Double top

Not Yet Submerged in Massecuite

3 – Single near pan wall

Vapour vs. Liquid: 6.6%

4 – Single near down take

Vapour vs. Liquid: 6.6%

Figure 5-9: Pan 1% full, beginning to boil

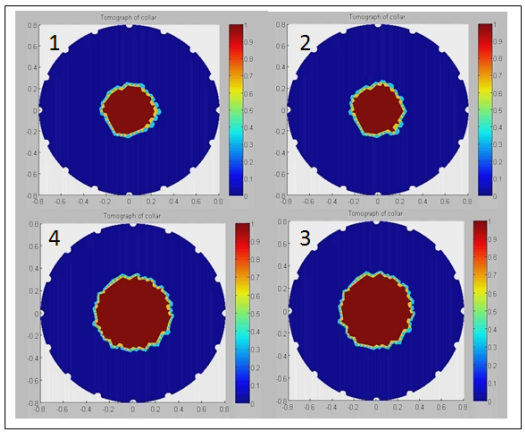

1 – Double bottom

Vapour vs. Liquid: 9.0%

2 – Double top

Vapour vs. Liquid: 9.2%

3 – Single near pan wall

Vapour vs. Liquid: 13.8%

4 – Single near down take

Vapour vs. Liquid: 13.6%

Figure 5-10: Pan at 5%

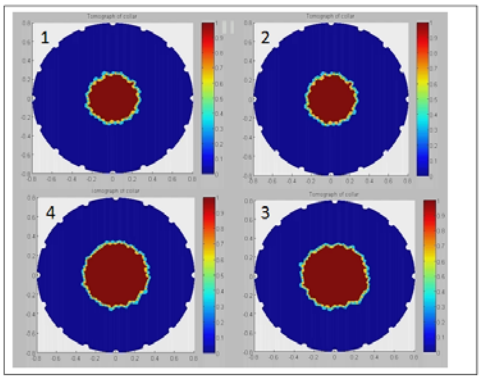

1 – Double bottom

Vapour vs. Liquid: 11.7%

2 – Double top

Vapour vs. Liquid: 10.8%

3 – Single near pan wall

Vapour vs. Liquid: 13.8%

4 – Single near down take

Vapour vs. Liquid: 13.6%

Figure 5-11: Pan at 18%

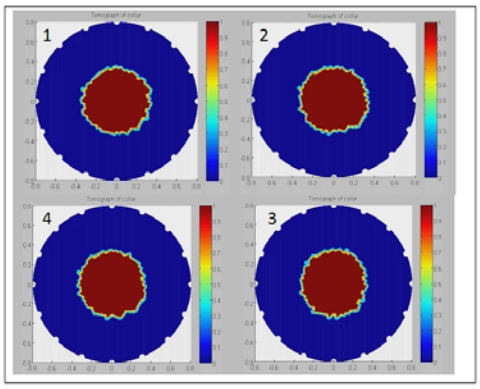

1 – Double bottom

Vapour vs. Liquid: 13.5%

2 – Double top

Vapour vs. Liquid: 13.4%

3 – Single near pan wall

Vapour vs. Liquid: 13.7%

4 – Single near down take

Vapour vs. Liquid: 13.6%

Figure 5-12: Pan at 53%

All zones continue boiling and show the same activity throughout the session - Figure 5-12 and Figure 5-13.

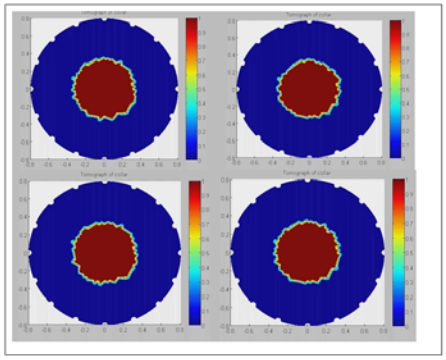

1 – Double bottom

Vapour vs. Liquid: 13.5%

2 – Double top

Vapour vs. Liquid: 13.6%

3 – Single near pan wall

Vapour vs. Liquid: 13.6%

4 – Single near down take

Vapour vs. Liquid: 13.7%

Figure 5-13: Pan at 87%

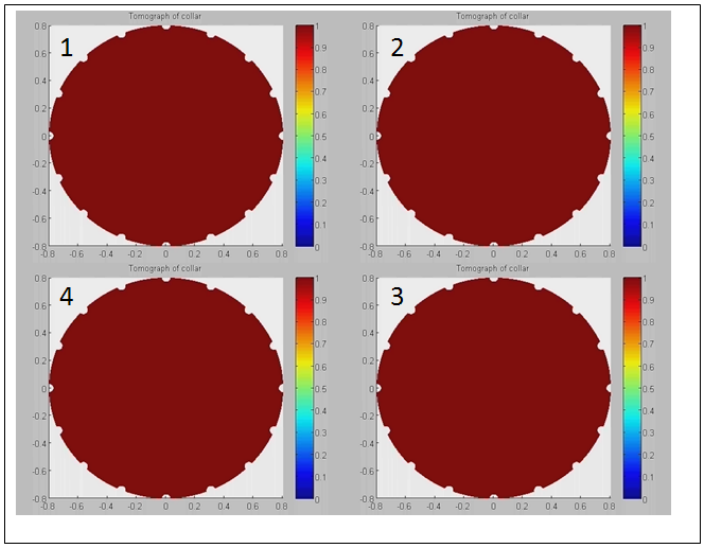

Figure 5-14: All zones empty after strike

After striking the pan all zones depicted empty phantoms - Figure 5-14. A graph showing the percentage vapours vs. liquid over the entire pan boil for all four of the sensor zones is shown in Figure 5-15.

These results show a significant difference from the first set of results, where the boiling was more typical as opposed to a single continuous bubble as shown in the above results, which indicate that the pan was boiling in the so-called 'slug regime' as discussed by Echeverri *et al* [**10**], which has previously only been observed in a laboratory environment. As the system can only operating at 5 frames s^{-1}, it is accepted that the slugs were travelling too fast through the tube and were also too long to differentiate between the slug of air in the centre of the tube and massecuite. The presence of the slug regime also indicates that the massecuite used for this test was of a high viscosity (>0.7Pa.s), as opposed to the first test where the boiling dynamics indicated a lower viscosity (<0.7Pa.s).

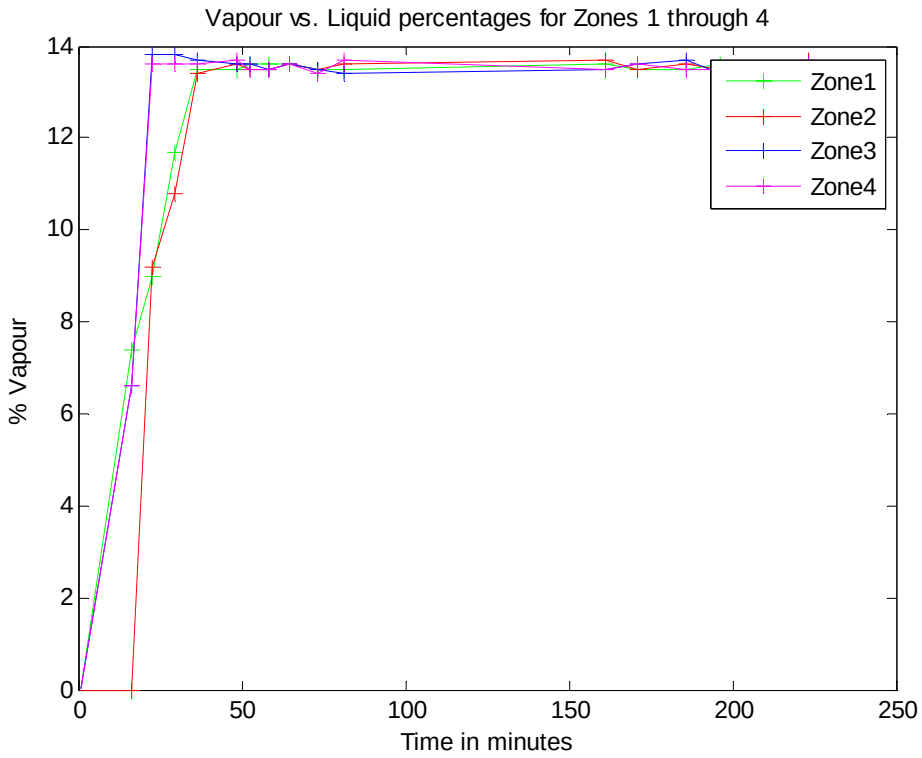

Figure 5-15: Graph of Liquid percentages vs. Percentage Vapour in tube for November 2008 Mill Test

Figure 5-15 shows the Percentage Liquid vs. Percentage Vapour graphs for all zones for the November 2008 test. All zones rise to a uniform liquid to vapour ratio which remains constant throughout the boil, which in turn indicates that the circulation within the pan was good.

5.2.4 October 2009

Readings were taken at the Maidstone Sugar Mill in Tongaat on Tuesday 20th October 2009 - (refer to Figure 4-8 for layout of collars within pan). A new collar design was used to ensure that firstly the readings would be as accurate as possible, and secondly that they would remain intact within the pan in order to make future experiments easier. Readings were taken regularly from the start of a boil up until the strike, and for part of the following boil.

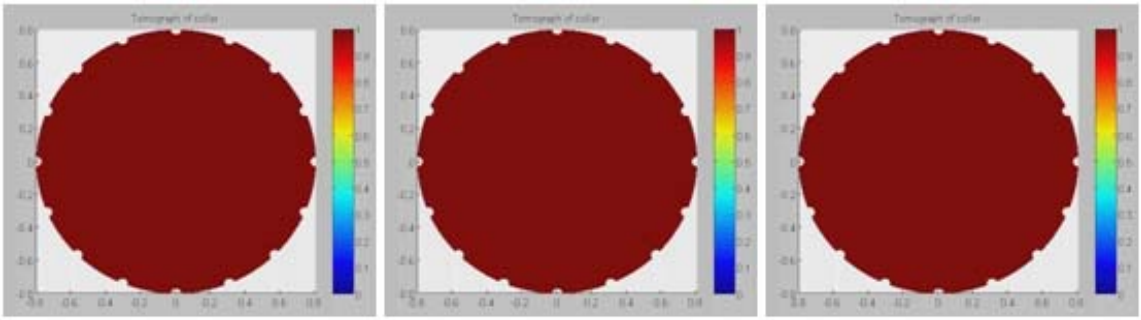

Figure 5-16: (left - right) Pan wall, halfway, and downtake collars when pan is empty. Atmospheric pressure.

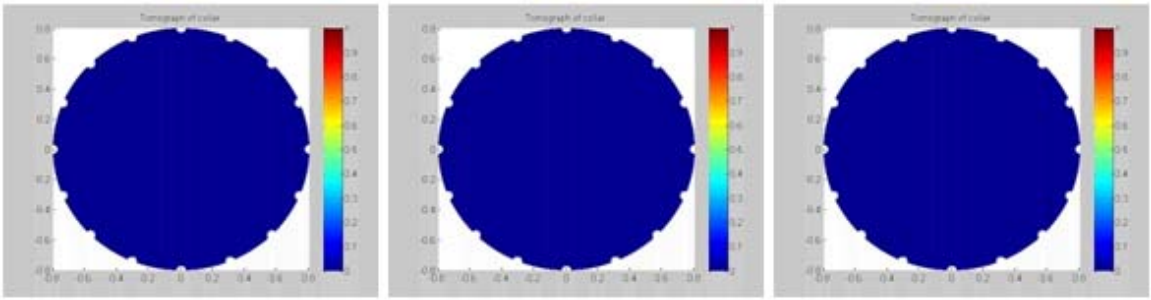

Figure 5-17: (left-right) Pan wall, halfway, and downtake collars at the end of boiling.

Vacuum breaking, all collars show no activity

As soon as the vacuum was broken all collars ceased to boil – showing how dependant the boiling process is on pressure levels.

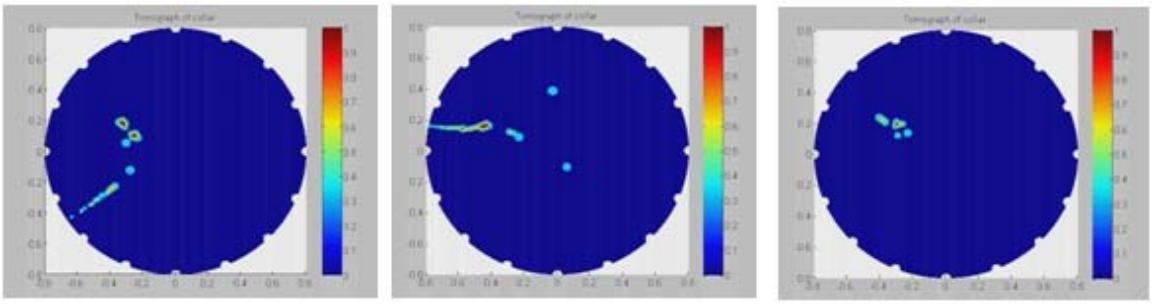

Figure 5-18: Steam on, beginning to boil - -78kPa

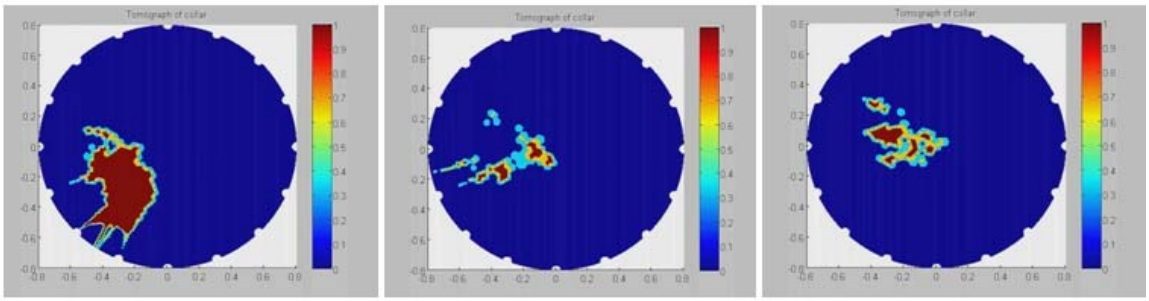

Figure 5-19: Increased activity (pan at 13% full, -79kPa)

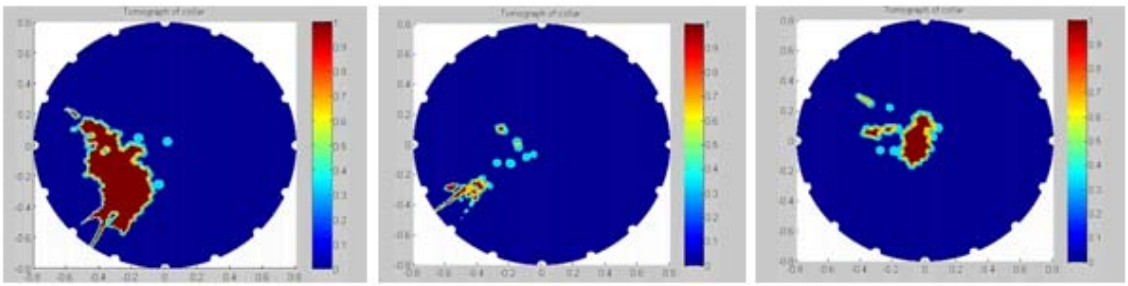

Figure 5-20: Boiling, 30% full, -80kPa

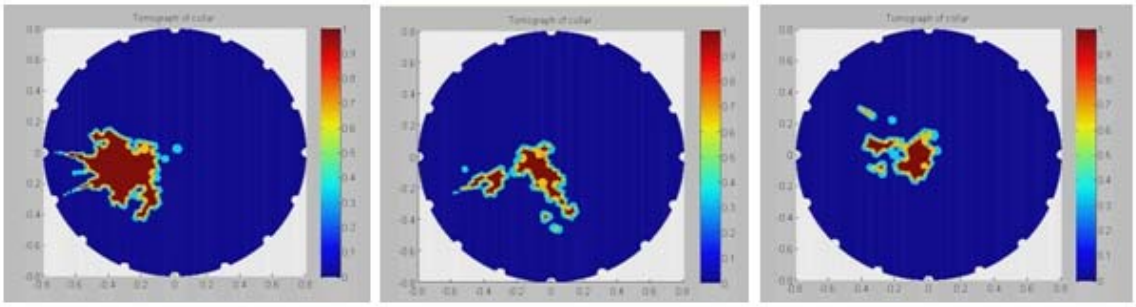

Figure 5-21: Boiling, 50% full, -80kPa

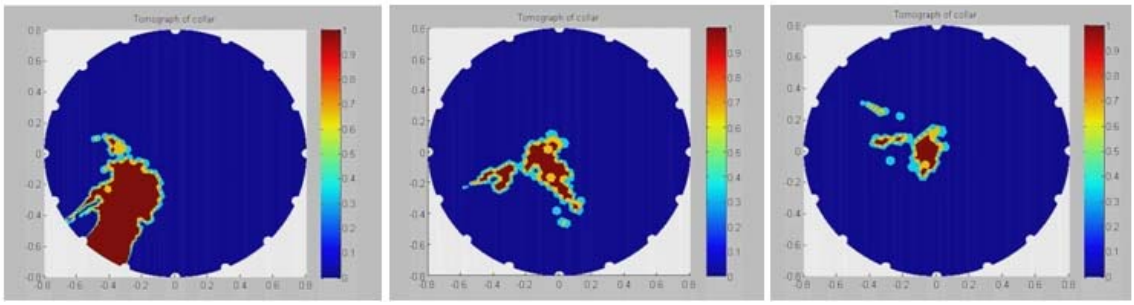

Figure 5-22: Boiling, 70% full, -79kPa

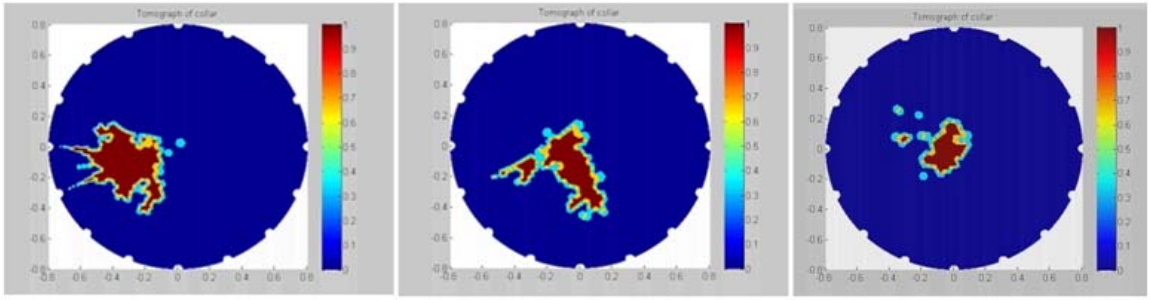

Figure 5-23: Boiling, 91% full, -81kPa

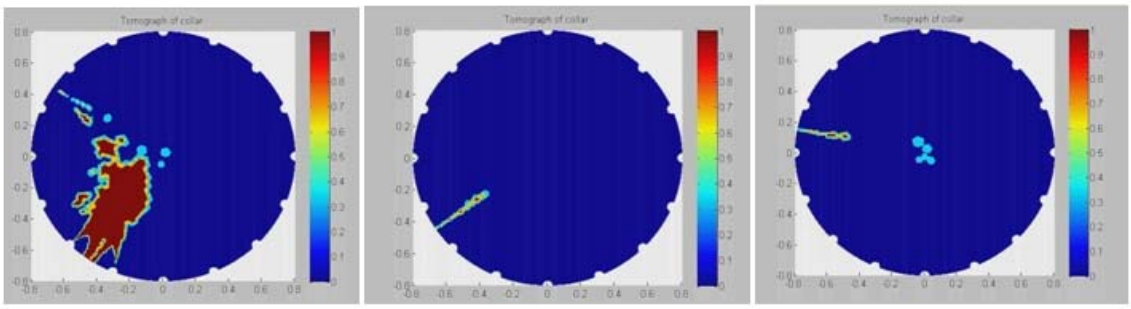

Figure 5-24: Immediately prior to strike (-80kPa, steam off but vacuum still on)

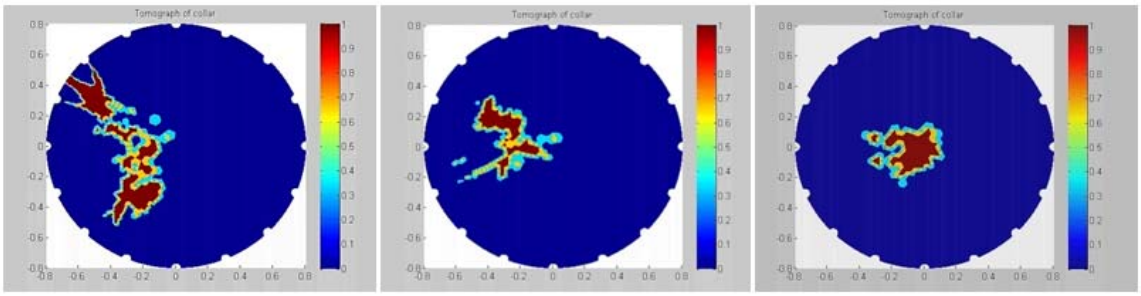

Figure 5-25: Pan striking

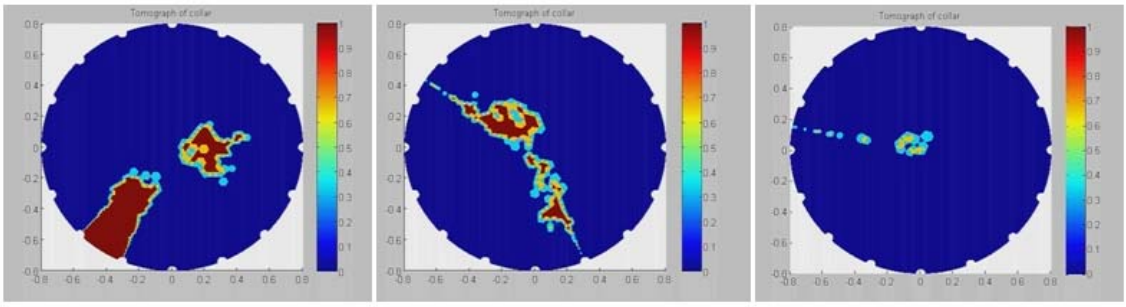

Figure 5-26: Pan beginning to boil again for next session (5% full, -77kPa)

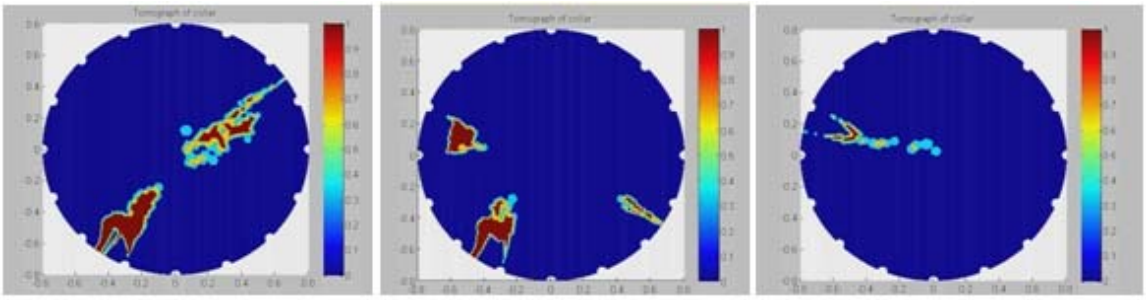

Figure 5-27: Boiling, 25% full, -81kPa

Throughout the boiling period the collar situated closer to the pan wall displayed consistently more activity than the other two collars. The collar next to the downtake also exhibited less activity. The absence of a slug regime for this test indicates that the massecuite used in this test was of a low viscosity (<0.7Pa.s).

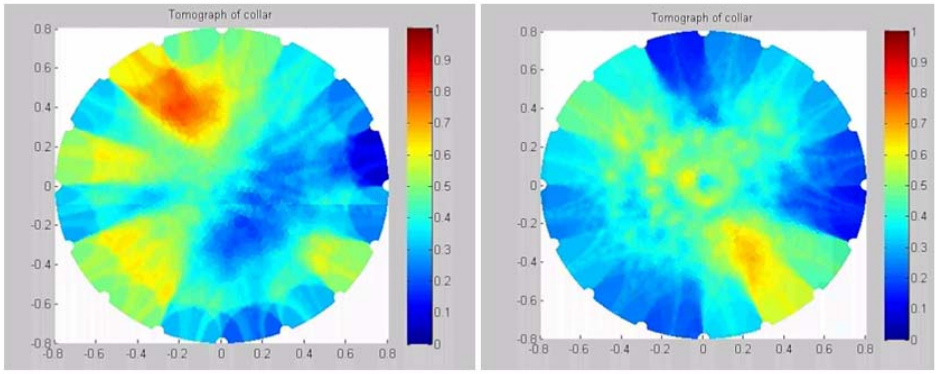

Figure 5-28: Raw data from mill

Figure 5-28 shows two examples of raw data obtained in the mill.

6. Future Work

The main aim of this project was to develop a system which could characterise boiling activity in a vacuum sugar pan via ERT images of tubes within the pan. The heat transfer characteristics from the steam to the massecuite can then be determined, as well as the uniformity of boiling within the pan. This was achieved, with the data being processed post-capture; hence the tomographical videos are generated 'off-line'. It takes approximately 1.5 seconds to generate a single image using Matlab (depending on system specifications), and in the mill environment this is sufficient as a single boiling session is in the region of three hours; several movies can then be made of various boiling stages and processed during the boil. Whilst not a requirement in terms of performance, real-time presentation of images depicting boiling would be useful to users in the field, especially if the system were to be adapted for use in other industries.

Matlab is not suited to real-time generation of images; it has too many overheads and is simply not fast enough. Hence some development work has been done in the Visual C# environment towards a real-time tomography solution. There is a local piece of hardware available which is C# compatible and is well suited to the tomography application, which renders both DasyLab and the DaqBook2001 obsolete.

Eagle Technologies [**17**] have a data acquisition board which is more ideally suited to tomography, and in particular real-time implementation: the USB 30B μDAQ. It contains 16 single-ended or 8 differential 14- bit analogue inputs with a maximum sampling rate of 250 kHz, and connects to the host PC via USB. The offline system generated 7 frames s^{-1} (i.e. 142ms is required to capture a single image), a figure limited by the nature of the capacitive massecuite. A system capable of capturing 500 fps would generate a switching frequency of 104 kHz, which would require a sampling frequency of at least 208 kHz according to the Nyquist principle. 500 frames s^{-1} is more than sufficient for viewing real-time tomography, and in the mill environment where the switching frequency is severely limited 7 frames $^{-1}$ would still be suitable for a real-time application.

C# is an ideal platform for real-time 'brute-force' image generation due not only to its speed when compared to Matlab, but also its ability to process and manipulate a data stream as it is being written to file – i.e. in 'real time'. Whilst not as fast as intrinsic-processing languages such as C or C++, it is still fast enough to generate a real-time image. Once this hurdle has been overcome, generating the images is simply a matter of converting the Matlab image generation code into the C# language as the reconstruction algorithm remains unchanged.

Due to the time pressures of the sugar industry's crushing schedule and the need to complete a successful test using collars which could withstand striking in the pan, the real-time component was not taken to completion. Mesh code and simulation data has successfully been implemented in the C# environment, and a new student has taken over from this point.

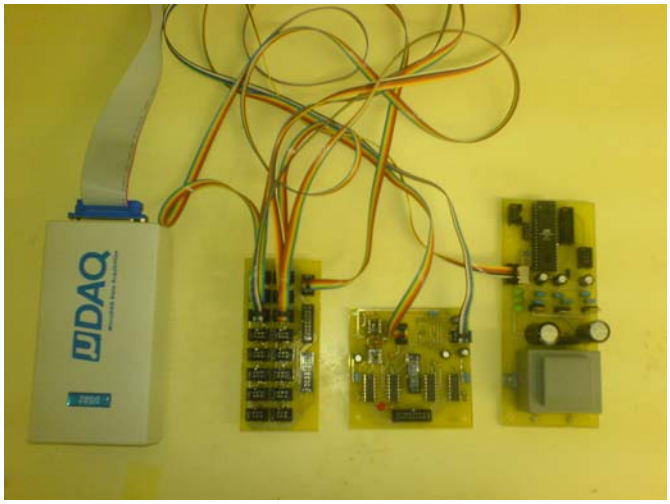

Figure 6-1: Hardware for real-time system: (left-right) USB 30B µDAQ, collar interface board, injection and multiplexing module, and control and power supply module

In order to produce a real-time system, the reconstruction algorithm, visual display to screen and Graphical User Interface (GUI) need to be implemented. Other methods could also be investigated, such as the opposite method for more sensitivity in the centre of the sensor zone. Implementing other methods would not require adaptation of hardware, as the microcontroller and multiplexing system is flexible and can be configured to any number of current injection scenarios.

7. Conclusions

The focus of this dissertation was to investigate tomography as a tool in the sugar industry. A prototype tomography system which could differentiate between areas of low vs. high conductivity, in particular with respect to the multiphase flow present in boiling calandria tubes in vacuum sugar pans.

All aspects of the system were designed and implemented; these included the mechanical interfaces, data acquisition modules and software algorithms which together produce images reflecting the dynamics within a phantom. The data acquisition modules comprise of an in-house designed electronic state machine, and the mechanical interfaces of tubular collars containing electrodes connected to the state machine via co-axial cabling. The software algorithm was developed in MATLAB using a Neighbourhood back-projection reconstruction technique.

Laboratory results have shown that the system functions accurately for a range of media, and results from tests in industry have detected various types of boiling dynamics, which help to better understand the operation, design and improvement of vacuum sugar pans.

Tests in the field at Maidstone Mill identified two different boiling modes; a ‘slug regime’ where high viscosity massecuite causes the bubbles to coalesce together and the massecuite and vapour travel together in ‘slugs’, and a ‘standard’ bubble formation in lower viscosity massecuite. The chemical engineers who design the pans can find this information extremely useful as uniform boiling and constant heat transfer is essential for optimum sugar production, and when new pans are designed the information describing the boiling dynamics of existing pans is invaluable.

Bibliography

[1] Adam Hilger, *Electrical Impedance Tomography*, J G Webster, Ed.: IOP Publishing, 1990.

[2] W R Breckon, "Image Reconstruction in EIT," 1990, PhD Thesis.

[3] E J Woo, O Kwon, J Y Lee, and J K Seo, Electrical Impedance Tomography and its applications, 2001, Korean University Collaboration.

[4] W Yin, N Holliday M Wang, "A highly adaptive electrical impedance sensing system for flow measurement," *Measurement Science and Technology*, p. 1884–1889, 2002.

[5] M Magnor and I Ihrke, "Adaptive grid optical tomography," *Graphical Models*, p. 484–495, 2006.

[6] Dr Steve Davis, Head of Prcess Engineering, SMRI, 2008.

[7] Dr David Love, Tongaat Hullets Design Engineer, 2009.

[8] B Lionheart, Seminar Series in Mathematics for Tomography, 2000, Lecture Notes.

[9] Adrian Boutelje, Adaptive Tomography Experiment, 2007.

[10] L F Echeverri, P W Rein, and S Acharya, "Measurements and CFD simulation of the flow in vacuum pans," *Proc. Int. Soc. Sugar Cane Technol.*, vol. 26, pp. 1341-1353, 2007.

[11] F A Jeglic and T M Grace, "Onset of flow oscillations in forced flow subcooled boiling," Lewis Research Center, Cleveland, USA, NASA Technical Note TN D-2821, 1965.

[12] A Borsic, Regularisation methods for imaging from electrical measurements, 2002, PhD, Oxford University.

[13] F Dickin and M Wang, "Electrical Resistance Tomography for Process Applications," *Measurement Science and Technology*, vol. 7, no. 3, pp. 247-260, 1996.

[14] M Vauhkonen, "Electrical impedance tomography and prior information," Kuopio

University, PhD Thesis 1997.

[15] C J Grootveld and A Segal, "Regularised modified Bewton-Rhapson technique applied to Electrical Impedance Tomography," *International Journal of Imaging and Technology*, vol. 9, pp. 60-65, 1997.

[16] M Wang et al., "A high-performance EIT system," *IEEE Sensors*, vol. 5, no. 2, pp. 289-299, April 2005.

[17] Eagle Technologies. [Online]. http://www.eagle.co.za/

[18] N J Avis and D C Barber, "Image reconstruction using non-adjacent drive configurations," *Physiological Measurement*, vol. 15, no. 2A, pp. A153-A160, 1994.

[19] C W L Denyer, Electronics for real-time and three dimensional electrical impedance tomographs, 1996, PhD, Oxford University.

[20] "Walsh Function Current Patterns and Data Synthesis for Electrical Impedance Tomography," *IEEE Transactions on Medical Imaging*, vol. 11, no. 4, pp. 554-559, 1992.

[21] I Frerichs, "Electrical Impedance Tomography (EIT) in applications related to lung and ventilation: a review of clinical and experimental activities," *Physiological Measurement* , vol. 21, pp. 1-21, 2000.

[22] Mike Spear, "Validating CFD with Tomography," *Process Engineering*, pp. 15-16, March 2003.

[23] G Nicholls, M Palm C Fox, Efficient Solution of Boundary-Value Problems for Image Reconstruction via Sampling, September 1999, University of Auckland.

[24] T York, "Status of Electrical Tomography in Industrial Applications," *Journal of Electonic Imaging*, vol. 10, pp. 608-619, 2001.

[25] T York, S Murphy, A Burnett-Thompson, and B Grieve, "An Accessible Electrical Impedance Imaging System," in *Proceedings of 4th World Congress on Industrial Process Tomography*, 2005.

[26] J L Wheeler, W Wang, and M Tang, "A comparison of methods for measurement of spatial resolution in two-dimensional circular EIT images," *Physiological Measurement*, vol. 23, no. 1, pp. 169-176, 2002.

[27] M Mollinari, B H Blott, S J Cox, and G J Daniel, "Optical imaging with adaptive mesh refinement in Electrical Impedance Tomography," *Physiological Measurement*, vol. 23, pp. 121-128, October 2001.

[28] S Artridge and M Schweiger, "A gradient-based optimisation scheme for optical tomography," *Optics Express*, vol. 2, pp. 213-226, 1998.

[29] D Isaacson, "Distinguishability of conductivities by electric current computed tomography," *IEEE Trans. Med. Imaging*, vol. 5, pp. 91-95, 1986.

[30] B H Blott, G J Daniell, and S Meeson, "Electrical impedance tomography with compensation for electrode positioning variations," *Phys. Med. Biol.*, vol. 43, pp. 1731-1739, 1998.

[31] A J Wilkinson, E J Randall, A Collins, and T M Long, "The design of an ERT system for 3D data acquisition and a quantitative evaluation of its performance," *Measurement Science and Technology*, p. 2088–2096, 2006.

[32] D C Barber and B H Brown, "Applied potential tomography," *Scientific Instruments*, 1984.

[33] O Isaksen, "A review of reconstruction techniques for capacitance tomography," *Measurement Science and Technology*, vol. 7, no. 3, pp. 325-337, 1996.

Appendix

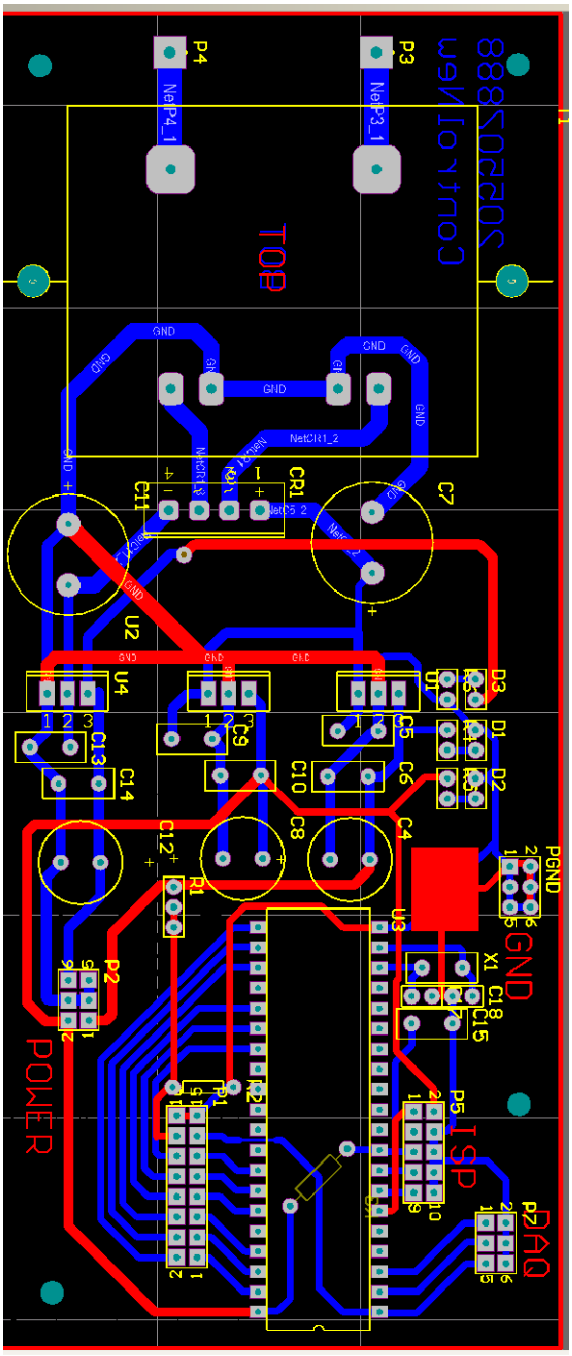

Figure 0-1:Control circuit schematic

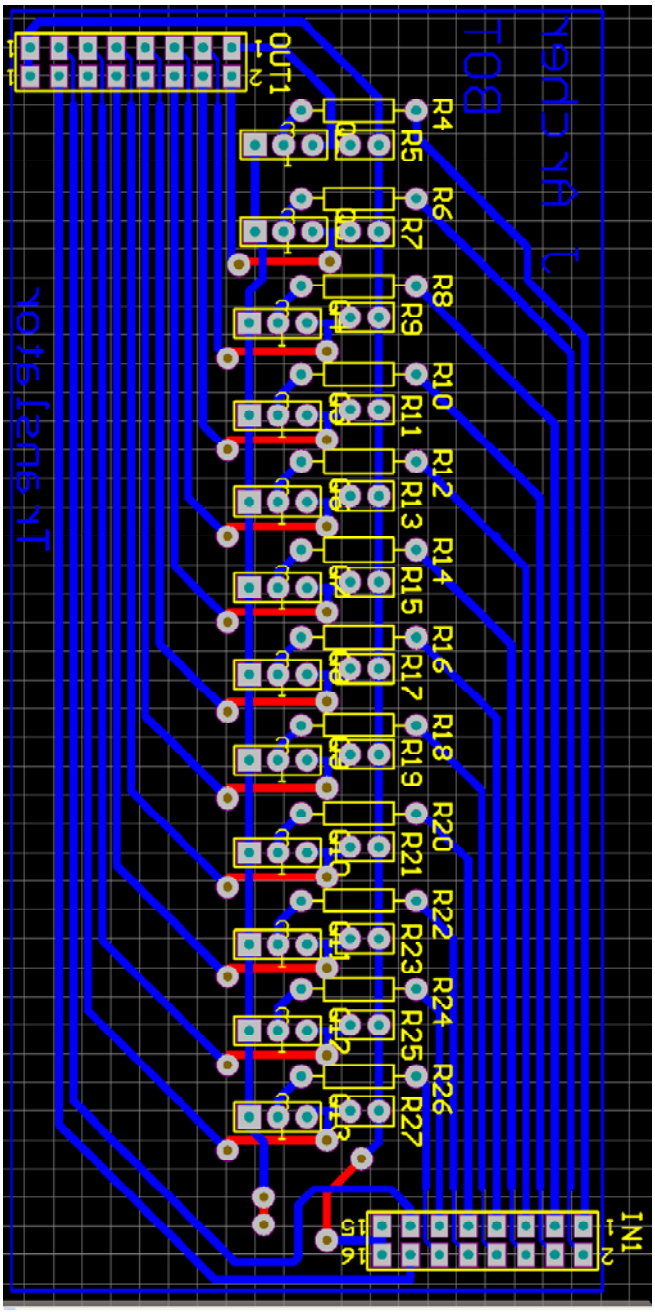

Figure 0-2: Logic level translator PCB

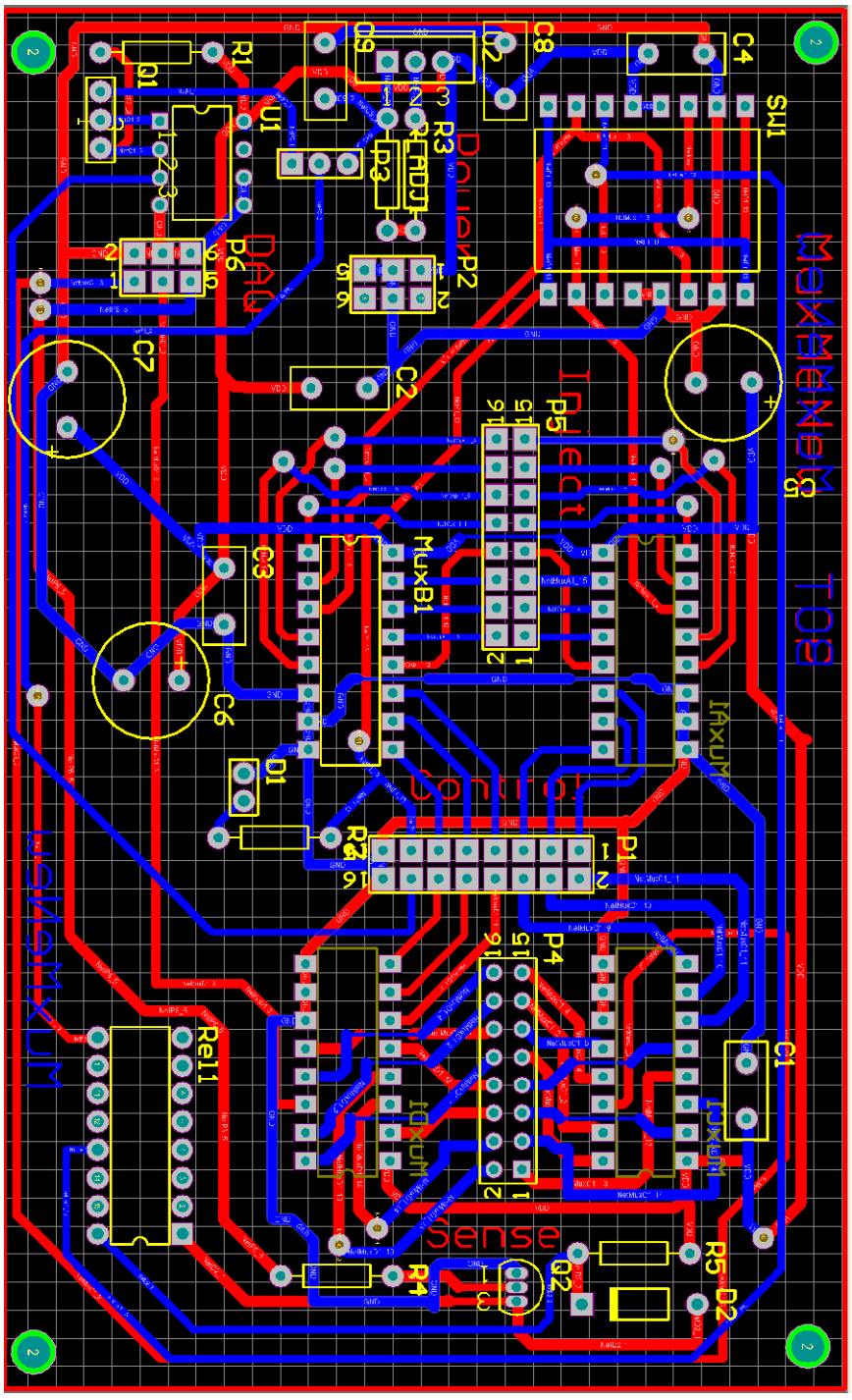

Figure 0-3: MuxMe PCB, Top Layer Tracks Blue and Bottom Layer Tracks Red